SNM1A (*DCLRE1A*) is required for the efficient repair of complex DNA breaks in human cells

Lonnie P. Swift[1], B. Christoffer Lagerholm[2, 5], Hannah T. Baddock[1], Malitha Ratnaweera[1], Blanka Sengerova[1, 6], Sook Lee[1], Helle D. Ulrich[3], Christian Renz[3], Dominic Waithe[2], Christopher J. Schofield[4] and Peter J. McHugh[1*]

[1]*Department of Oncology, MRC-Weatherall Institute of Molecular Medicine, University of Oxford, John Radcliffe Hospital, Oxford OX3 9DS, UK*
[2]*Wolfson Imaging Centre, MRC-Weatherall Institute of Molecular Medicine, University of Oxford, John Radcliffe Hospital, Oxford OX3 9DS, UK*
[3]*Institute of Molecular Biology gGmbH (IMB), Ackermannweg 4, 55128 Mainz, Germany*
[4]*Chemistry Research Laboratory, Department of Chemistry and the Ineos Oxford Institute for Antimicrobial Research, University of Oxford, Oxford, OX1 3TA, UK*

Correspondence: peter.mchugh@imm.ox.ac.uk

Present Addresses:
[5]*Kennedy Institute of Rheumatology, University of Oxford, Roosevelt Drive, Oxford, OX3 7FY, UK*
[6]*Institute of Organic Chemistry and Biochemistry of the Czech Academy of Sciences. Flemingovo náměstí 542/2 160 00 Praha 6. Czech Republic*

Abstract
DNA breaks, in particular double-strand breaks (DSBs), produced by radiation and radiomimetic agents are amongst the most toxic forms of DNA damage, in part because they are associated with extensive oxidative chemical modification at the break termini. Prior to the completion of DSB repair, the chemically modified termini associated with radiation-induced damage must be removed. A number of DNA processing enzymes have been implicated in the processing of these 'dirty ends', but our knowledge of this process remains limited. Here, we demonstrate a role for the 5'-3' exonuclease SNM1A in this process. Cells disrupted for SNM1A are sensitive to radiation and radiomimetic agents and show defects in the resolution of the lethal DSB damage they induce. SNM1A is recruited and retained to the sites of complex DNA damage *via* the concerted action of three highly conserved interaction domains the PBZ, UBZ and PIP box, mediating interactions with poly-ADP-ribose chains, PCNA and the ubiquitinated form of PCNA, respectively. Consistent with its unprecedented capacity to digest DNA containing a wide range of chemically modified nucleotides, we found that SNM1A can resect DNA containing oxidative lesions representative of those induced by radiation damage at break termini. Taken together, our work reveals a crucial role for SNM1A in the repair of toxic DNA breaks.

Introduction

DNA double-strand breaks (DSBs) are known to be one of the most cytotoxic forms of DNA damage, where a small number of unrepaired breaks are potentially lethal[1]. In human cells, the majority of these breaks will ultimately be resolved by one of two major pathways, non-homologous end-joining (active from G1- through to the G2-phase of the cell cycle) or homologous recombination (which becomes active as cell traverse S-phase)[2]. However, prior to the completion of DSB repair, any chemically modified nucleotides or aberrant structures must be removed from the break-ends. This is especially important for DSBs induced by ionising radiation (IR) or radiomimetic drugs, which include bleomycin and related agents, as these are associated with extensive (mostly oxidative) modification to DNA at the break termini[3,4]. A number of nucleases have been implicated in processing such ends, including tyrosyl DNA phosphodiesterase (TDP1)[5], polynucleotide kinase (PNK)[6], aprataxin[7-10] and Artemis/SNM1C (discussed below)[11,12]. TDP1 removes the 3'-phosphoglycolate ends that constitute approximately 10% of the termini produced by IR[13]. PNK is capable of removing 3'-phosphate groups and adding phosphates to 5'-hydroxyl moieties in preparation for end ligation[6], modifications that are again associated with oxidation reactions following IR. Aprataxin catalyses a deadenylation reaction to release DNA Ligase IV during abortive ligation reactions during NHEJ, removing the associated AMP group[14].

The SNM1A 5'-3' exonuclease encoded by the *DCLRE1A* gene is a member of a highly-conserved family of nuclease present from yeast through to humans[15]. This family is characterised by a conserved metallo-β-lactamase (MBL) structural motif proximal to a family-identifying β-CASP (CPSF-Artemis-SNM1A-Pso2) motif that fold together to form the enzymatic active site[16]. Human cells express three MBL-β-CASP nucleases paralogues, SNM1A, SNM1B (also known as Apollo) and SNM1C (Artemis)[16]. SNM1A plays a key role in DNA interstrand crosslink repair (ICL repair) in yeast through to human cells, where a role in the replication-coupled pathway of ICL repair in mammalian cells is mediated through the interaction of SNM1A with PCNA *via* its PCNA interacting protein (PIP) motif as well as an interaction *via* a N-terminally located ubiquitin-binding zinc finger (UBZ) with the monoubiquitinated form of PCNA[15,17,18]. The DNA repair role of SNM1B/Apollo remains poorly resolved, but this factor has a well-described role in the process of newly-synthesised telomere leading-strands in order to maintain the structure of telomere termini[19]. Both SNM1A and SNM1B/Apollo are 5'-3' exonucleases[20]. SNM1C/Artemis has a distinct biochemical profile, with some 5'-3' exonuclease activity, but upon association with DNA-PKcs (the catalytic subunit of the NHEJ factor DNA-PK), acquires 5'-3' endonuclease activity with the capacity to open DNA hairpins and also to remove overhangs at or unpaired regions at DNA termini containing chemical damage and aberrant structures[12,21]. For this reason, Artemis is known to play a key role in V(D)J, where it removes RAG-generated hairpin intermediates, but also in the processing of DNA breaks bearing modified termini including oxidised nucleotides and other lesions induced by IR as part of the NHEJ pathway.

Employing genome-editing techniques we have created cell lines disrupted for SNM1A. While these cells display the expected sensitivity to DNA crosslinking agents, screening for DNA damage sensitivities more generally revealed sensitivity to radiation and radiomimetic agents. This striking -- and unanticipated -- observation led to us to characterise a repair response in SNM1A-deficent cells, which is likely underpinned by the exceptional capacity of

SNM1A to process DNA substrates that contain nucleotides that have been subject to gross chemical and structural alterations.

Results

SNM1A$^-$ cells show a profound sensitivity to radiometric damage

In order to comprehensively examine the phenotype of human cells disrupted for SNM1A we utilised both Zinc-Finger Nuclease (ZFN)[22] and CRISPR-Cas9[23] technology to generate SNM1A$^-$ cells. Initially, we employed ZNF constructs targeting the first exon of SNM1A. A putative U2OS SNM1A disruptant clones was identified, containing a 22-nucleotide deletion in exon 1, producing a frameshift and premature stop codon distal from the deletion site (Suppl. Table 1) and SNM1A protein could not be detected by immunoblotting (Fig. 1A). To examine the DNA damage response defects in cells lacking SNM1A, we treated these cells with a broad range of genotoxic agents and determined their survival relative to their parental U2OS cells in clonogenic survival assays. As expected from previous work, SNM1A$^-$ cells were sensitive to the crosslinking agents cisplatin and SJG-136, confirming the important role SNM1A plays in removing ICLs (Fig. 1A and 1B). Moreover, loss of SNM1A accounts for sensitivity of this cell line to cisplatin, since stable reintroduction of EGFP-SNM1A into this cell line restored the cisplatin sensitivity of the SNM1A$^-$ cells to near wild-type levels (Fig. 1A). An absence of increased sensitivity was observed across a broad range of genotoxins, including hydrogen peroxide (H_20_2), the toposiomeraes 1 inhibitor Campothecin and formaldehyde for the SNM1A$^-$ cells relative to the parental U2OS cells (Suppl. Fig. 1B, C, D). Sensitivity to UVC irradiation was observed, possibly as a consequence of the rare ICLs induced by this form of damage (Suppl. Fig. 1A). Most strikingly, for the radiomimetic drug Zeocin, a dramatic sensitisation was observed for the SNM1A$^-$ cells that again could be suppressed by stable complementation with the EGFP-SNM1A (Fig. 1C). Since the principal genotoxic lesion induced by Zeocin is DSBs associated with chemically modified termini[24], we also assessed the sensitivity of the SNM1A$^-$ cells to ionising radiation (IR) which induces related forms of damage (Fig. 1D). Sensitivity to IR was observed, although the overall increase in sensitisation was lower than for Zeocin. Together these results suggest a role for SNM1A in the repair of the major cytotoxic lesions induced by Zeocin and IR, namely DNA breaks associated with chemically modified termini. In order to confirm our findings by independent means, we employed CRISPR-Cas9 technology to target a sequence in the first exon of SNM1A in HEK293T cells (Suppl. Table 1). Again, we were able to identify clones that harboured disruptions that produce a frame shift a distal introduction of a premature stop codon, and these cells do not express SNM1A as determined by immunoblot (Fig. 1E). Like the U2OS clones described above, these cells are sensitive to the ICL inducing agents, cisplatin and SJG-136 (Suppl. Fig. 2B), and again also demonstrate a striking sensitivity to Zeocin (Fig. 1E).

SNM1A$^-$ cells are defective in the repair of radiation and radiomimetic damage

As SNM1A is a 5'-3' repair exonuclease, a plausible explanation for the sensitivity of SNM1A cells to Zeocin and IR is a defect in the processing of the major toxic DNA lesion induced by these agents, complex DNA breaks, where complex DSBs represent to key cytotoxic lesion. In order to determine whether SNM1A$^-$ cells exhibit the hallmarks of a DSB repair defect following challenge with Zeocin and IR, we initially employed pulsed field gel electrophoresis with the aim of directly detecting DSBs and monitoring their resolution. However, in the cell lines employed we found that the doses of Zeocin or IR required to permit detection of DSBs

were too high for repair to be monitored in the parental U2OS or HEK293T cells. Consequently, we moved to monitoring the dynamics of γH2AX and 53BP1 foci, which are sensitive markers of DSB induction[25,26]. In U2OS cells, following treatment with Zeocin or IR, γH2AX and 53BP1 levels peaked within 2 hours, consistent with previously reported dynamics and were largely resolved within 24 hours (Fig. 1F, 1G and 1H). However, in SNM1A$^-$ cells a substantial fraction of γH2AX and 53BP1 foci persisted at 24 hours. Employing IR as the DSB-inducing agent confirmed marked delay γH2AX foci resolution in SNM1A cells (Fig. 1H). Moreover, analysis of cell cycle progression following Zeocin treatment (0.1 mg/mL) demonstrated that parental (U2OS) cells only transiently slowed and arrested, whereas the SNM1A cell accumulated in the G2/M phase of the cell cycle for up to 48 hours, characteristic of cells accumulating of unrepaired DSBs (Fig. 1I, Suppl. Fig. 2). Importantly, reporter assays designed to reveal overt defects in NHEJ or HR induced by the 'clean' DSBs produced by homing endonucleases revealed no defect in SNM1A$^-$ cells (Suppl. Fig. 3A and 3B), where cell disrupted for XRCC4 and depleted for BRCA2, respectively, acted as positive controls for defects in these processes[27,28]. Interestingly, a slightly elevated level of HR was observed for SNM1A$^-$ cells, implying a potential minor role in DSB repair pathway utilisation at clean breaks, but no necessary role. Therefore, only DNA DSBs associated with complex, chemically altered termini, such as those induced by radiation and radiomimetics, depend upon SNM1A for their repair.

Consequently, we examined whether SNM1A is recruited to the sites of Zeocin-induced DSBs, employing cells that stably express a functional N-terminally EGFP-tagged form of SNM1A, expressed at levels not substantially greater than the endogenous protein (Fig. 1A). Employing 53BP1 as a marker for DSB induction and localisation, we observed that upon Zeocin treatment the majority of 53BP1 foci are closely colocalised to EGFP-SNM1A foci (Fig. 2A). High resolution images revealed that these colocalising foci exhibit a pattern of staining where SNM1A localises immediately adjacent to 53BP1 foci. (Fig. 2B).

Together, this data demonstrates that SNM1A plays an important role in protecting cells from complex DSBs, that efficient resolution requires of complex DSBs requires SNM1A, and that SNM1A localises at the sites of complex DSBs.

The PBZ, UBZ and PIP box act in concert to recruit SNM1A to the site of complex DNA breaks

The N-terminus of SNM1A contains both predicted ligand interaction motifs, including a putative poly-ADP-ribose (PAR)-binding zinc finger (PBZ)[15,29], a ubiquitin-binding zinc finger (UBZ)[15,30] which is involved in the localisation of SNM1A to ICLs in S-phase through mediating interaction with ubiquitinated PCNA and a PIP (PCNA interacting peptide) box[15,31] (Fig. 3A, and sequence alignments shown in Suppl. Fig. 4). However, the direct interaction of these motifs with any of the predicted ligands has yet to be tested. As structural insight into SNM1A's non-catalytic N-terminus is currently lacking due to its overall intrinsic disorder, we therefore predicted the architectures of the UBZ and PBZ domains, and PIP box using the AlphaFold computational model. These predictions aligned well with previously solved structures of these domains. The predicted SNM1A UBZ domain was structurally similar to RAD18's UBZ[32], barring a helical shift in the expected Zn^{2+} coordinating residues of its C3H1-type zinc finger (Fig 3B, top left panel); the predicted SNM1A PBZ domain closely matched the PBZ of APLF[33] and two critical PBZ residues C155 and C161 could be predicted to coordinate Zn^{2+} (Fig 3B, top right panel); the PIP box prediction for SNM1A agreed strongly with the (tight-

binding) PIP box of P21/WAF1[34], with critical residues Q556, I559, Y562 and F563 lying close to their expected grooves within PCNA (Fig 3B, bottom panel).

To address these ligand interactions experimentally, we designed and produced a series of N-terminally GST-tagged peptides containing the PBZ, UBZ or PIP box motifs and tested their capacity to binding (pull down) purified PCNA, purified lysine 164 ubiquitinated ($PCNA^{Ub}$) or PAR chains. This revealed that wild-type PIP box peptides were fully competent to bind to the PCNA and $PCNA^{ub}$, respectively, whereas a peptide containing substitutions at conserved residues in the relevant binding motifs, a PIP box (Y562A, F563A double substitution) did not pull down PCNA or $PCNA^{ub}$. While a GST peptide spanning the UBZ and PBZ motifs could not pull down native PCNA, a small quantity of $PCNA^{ub}$ was pulled down by this peptide, consistent with the UBZ4 motif having the capacity to interact with ubiquitinated proteins. A peptide harbouring predicted ligand binding mutations in the UBZ (C125F substitution) did not pull down $PCNA^{ub}$ (or PCNA) implying that indeed the residues mutated play a key role in mediating the interaction with $PCNA^{ub}$. Likewise, peptides representing the wild-type PBZ and UBZ motif were able to bind PAR chains in a dot-blot analysis, whereas those mutated for key predicted interacting resides in the PBZ (C155A, C161A) or doubly mutated for residues in both the PBZ and UBZ were not, where purified APLF, an established PBZ-containing protein[29], acted as a positive control.

Having confirmed that the PBZ, UPZ and PIP box mediate the predicted interactions *in vitro*, we sought to determine the potential role of each of these, in turn, to the recruitment of SNM1A to complex DSBs. Cells expressing forms of EGFP-SNM1A that ablate ligand interactions with PAR-chains, ubiquitin and the PIP box, respectively (EGFP-$SNM1^{PBZ}$; double C155A, C161A substitution: $SNM1A^{UBZ}$; C125FSNM1A^{PIP}; Y562A, C161A double substitution) were expressed in U2OS cells and the induction of SNM1A foci that co-localised with 53BP1 following Zeocin treatment determined (Fig. 4A and B, quantified in Fig. 4C). As before, wild-type EGFP-SNM1A protein colocalised 53BP1 following Zeocin treatment, and this localisation was independent of SNM1A enzymatic activity, since cells expressing a form of the protein containing nuclease-inactivating mutations (harbouring a D736A substitution, here denoted $SNM1A^{NI}$) was also recruited to the sites of Zeocin DSBs. Examination of the capacity of $SNM1A^{PBZ}$, $SNM1A^{UBz}$ and $SNM1^{PIP}$ variants revealed that only $SNM1A^{PIP}$ exhibited a trend in reduction in recruitment to Zeocin-induced DSBs that colocalised with 53BP1, although this was not statistically significant due to the wide range of foci observed in the cell population (Fig. 4C).

We therefore sought a more sensitive, dynamic and quantitative method to assess the relative contribution of ligand-binding motifs (PBZ, UBZ and PIP) in the localisation and retention of SNM1A to complex DSBs. Here, we turned to laser microirradiation using a 405 nm laser in the absence additional photosensitisers. Direct 405 nm laser irradiation is known to induce a high yield of single- and double-strand breaks associated with chemically modified termini, acting as the preferred surrogate for the damage induced by ionising radiation and radiomimetic drugs[35]. Examination of the kinetics of recruitment of either stably or transiently expressed EGFP-SNM1A in these cells revealed a rapid accumulation of EGFP-SNM1A at damage sites, becoming maximal within ~10 minutes of irradiation, kinetics typical of DSB repair factors (Fig. 5A and 5B). Moreover, the EGFP-SNM1A foci in the damage tracks again colocalised with the 53BP1 foci produced, confirming that this microirradiation technique

employed produces DSBs (Fig. 5A). Having established a system to evaluate the dynamics of EGFP-SNM1A at the sites of complex DSBs, we first examined inactivation of catalytic active site of SNM1A impact on recruitment dynamics. As with its ability to form foci following Zeocin damage, the EGFP-SNM1A^{NI} protein (SNM1A^{D736A}) was recruited to the laser stripes with kinetics indistinguishable to the wild-type protein, confirming that the catalytic activity of SNM1A is mechanistically separable from its recruitment and retention at complex DNA breaks (Fig. 5B, C). We also determined whether there was any cell cycle phase dependency on the recruitment of EGFP-SNM1A to complex breaks. EGFP-SNM1A was rapidly recruited to laser induced damage in G1-, S- and G2-phase cells (Fig. 5D, E). This implies a role for SNM1A in processing complex DNA breaks sustained throughout the cell cycle.

The PBZ, UBZ and PIP box collectively mediate recruitment and retention of SNM1A at complex breaks

Armed with a method for analysing SNM1A recruitment dynamics to complex DNA breaks, we sought to determine more closely define roles of the UBZ, PBZ and PIP box motifs. For both the SNM1A^{PBZ} and SNM1A^{PIP}, a delayed recruitment was observed and these proteins also never achieved the same local concentration at the laser site observed for the wild-type form (Fig. 6B, C). By contrast, the SNM1A^{UBZ} exhibited a near-normal initial rate of recruitment, never reaching the levels observed for the wild-type form, and then a gradual loss from the laser sites (Fig. 6B, C). Consistent with the marked reduction in Zeocin-induced foci colocalising with 53BP1 following mutation of the PIP box, SNM1A^{PIP} exhibited the most dramatic defect in laser stripe recruitment, suggesting that PCNA interaction is particularly important for SNM1A recruitment complex breaks (Fig. 6B, C). Together, therefore, our data implies a key role for the PIP box in the initial recruitment of SNM1A to laser damage, where the PBZ also makes a contribution to initial recruitment, and that the UBZ in stabilising the recruited protein at complex breaks.

We therefore sought to examine the kinetics of PCNA recruitment to the complex DSBs produced by Zeocin and those produced by the 405 nm laser, creating a cell line that stably expressed both EGFP-SNM1A and an anti-PCNA RPF-tagged nanobody[36] (Chromobody®, anti-PCNA VHH fused to red fluorescent protein). Employing this we could observe that PCNA is recruited to the sites of Zeocin-induced foci and to the sites of laser stripes, where it colocalises with EGFP-SNM1A and 53BP1 (Suppl. Fig. 5A). Moreover, examination of the kinetic of recruitment of PCNA to the laser stripes demonstrated that recruitment PCNA precedes EGFP-SNM1A arrival by several minutes (Suppl. Fig. 5A and 5B). This data is collectively consistent with a key role for PCNA in attracting EGFP-SNM1A to the sites of complex DNA breaks.

To examine the role of the UBZ further, we examined the recruitment kinetics of EGFP-SNM1A in cells depleted for the key E3 ubiquitin ligases involved in DSB repair. These include RAD18 (which is an established E3 ligase for the ubiquitination of PCNA[37], where PCNA^{ub} can associate with the SNM1A UBZ *in vitro*, Fig. 3C, D), RNF8 and RNF168 which mono- and poly-ubiquitinate histone H2A, respectively, in response to DSBs. Depletion of the these three E3 ligases using siRNA revealed that only depletion of RAD18 impacted in SNM1A recruitment to laser damage, and the defect was kinetically similar from mutation of the UBZ domain since it led to wild-type-like initial recruitment kinetics of SNM1A to the stripes, but lower overall levels of accumulation with a gradual loss of retention at these sites (Suppl. Fig 5C). The only

known target of Rad18 E3 ligase activity is the lysine 164 residue of PCNA. However, we were not able to detect the monoubiquitination of this residue by immunoblotting in whole cell extracts, using a ubiquitin-specific antibody raised against this epitope, likely because the fraction of PCNA which is ubiquitinated in these cells is extremely small. Nonetheless, a functional ubiquitin response is clearly required for the efficient recruitment and retention of SNM1A at the sites of laser damage, since pre-treatment of cells with MG132, an agent that exhausts the cellular free ubiquitin pool through proteosome inhibition[38], also dramatically reduced recruitment of EGFP-SNM1A to laser stripes (Suppl. Fig. 5D).

To examine the interplay and interdependence of the three key conserved motifs involved in SNM1A break localisation, we next created combinatorial double-mutations in the PBZ and UBZ, PBZ and PIP box, UBZ and PIP box and a form of SNM1A triply mutated in the PBZ, UBZ and PIP box. Analysis of the dynamics of recruitment and retention of the double and triple mutated forms of SNM1A revealed that mutation of either the PBZ or UBZ motifs together with the PIP box essentially eliminated SNM1A recruitment to and retention at laser stripes, and, mutation of the PBZ and UBZ drastically reduced recruitment and retention of EGFP-SNM1A to stripes. Accordingly, mutation of all three motifs eliminated recruitment (Fig. 6D). To further explore and confirm a role for the PBZ in the recruitment of SNM1A to complex breaks, we exploited a PARP inhibitor, Olaparib which competitively inhibits PARP1 and also produces PAR chain-shielding in cells through trapping the PARP enzyme during its catalytic cycle[39]. Pre-treatment of cells with Olaparib led to a reduction in rate of recruitment of EGFP-SNM1A to sites of laser damage (Fig. 6E). Combining Olaparib treatment with the EGFP-SNM1A^{PIP} led to an abrogation of recruitment and retention reminiscent of the double substitution mutation of the PBZ and PIP motifs (Fig. 6F). This suggests that interaction with PAR chains is important for efficient initial recruitment of SNM1A to laser damage. Together these results demonstrate that several conserved motifs orchestrate the initial recruitment (PBZ and PIP) of SNM1A to complex breaks and that the UBZ is important for SNM1A retention at these breaks, most likely *via* an association of PCNA^{ub}.

Since multiple interacting motifs in SNM1A act in concert to recruit and retain SNM1A at the sites of complex DNA damage, we asked whether or not interactions with their cognate ligands impacts on the exonuclease activity of SNM1A. Although the core catalytic domain of SNM1A is formed by the C-terminally located MBL-β-CASP fold, we wanted to rule out the possibility that the N-terminal motifs that regulate the damage localisation of SNM1A (PBZ, UBZ and PIP) of SNM1A impact on the activity of the protein. Here, we used the kinetically preferred substrate of SNM1A[40], a single-stranded 20-nucleotide oligonucleotide, bearing as 5′-phosphate group and radiolabelled at its 3′-end. When incubated with full-length SNM1A purified from human cells harbouring the same motif substitutions utilised in our preceding cell biology studies all forms of the protein retained comparable nuclease activity (Suppl. Fig. 6A). We therefore tested the impact of PCNA and PAR chains on the activity of full-length SNM1A protein. Titration of PCNA followed by analysis of the digestion activity over a time course of one hour revealed that PCNA did not enhance the activity of SNM1A, and in fact some decrease in digestion was observed (Suppl. Fig. 6B). In order to determine whether this was a direct effect mediated by the interaction of PCNA and SNM1A, we repeated this experiment with a N-terminally truncated form of SNM1A (ΔN-SNM1A) that retains the MBL-β-CASP fold (and therefore exonuclease activity), but lacks the PIP box. ΔN-SNM1A activity was also reduced in the presence of PCNA (Suppl. Fig. 6C) suggesting that the perturbation of

nuclease activity in the presence of PCNA interaction is most likely the result of reduced SNM1A access to the 5'-terminus of the DNA substrate in the presence of PCNA. Next, we employed the system first utilised in Fig. 2B to produce PAR chains *in situ* by pre-incubating poly-ADP-ribose polymerase with NAD and the DNA substrate with subsequent addition of purified full-length SNM1A to the reaction. The activity of SNM1A was not modulated the presence of PAR chains (Suppl. Fig. 6D). Together our biochemical analysis suggest that the interactions mediated by the PBZ, UBZ and PIP box are principally important for recruiting retaining SNM1A DNA damage, rather than modulating the activity of the enzyme.

SNM1A can process DNA containing oxidised lesions

Finally, we asked whether SNM1A is capable of processing DNA containing lesions relevant to the repair of complex DNA breaks, by analogy with its established role of resecting DNA containing ICLs. Using a 20-mer oligo nucleotide that contains an 8-oxoguanine (8-oxoG) residue, one of the major oxidative lesions induced by radiation and radiomimetic drugs at complex breaks[41], located centrally, or at its 5'-terminus. Incubation of these substrates with ΔN-SNM1A revealed that the exonuclease activity of the protein was able to traverse the lesion without pause or arrest (Fig. 7A). This striking activity stands in stark contrast to that of human Exonuclease 1, one of the major exonucleases involved in performing DNA extensive end resection in preparation for homologous recombination, which is quantitatively arrested by the presence of an 8-oxoG lesions regardless of whether it is located terminally or centrally in the substrate (Fig. 7A). We next examined whether SNM1A is able to process DNA substrates containing Zeocin-induced DNA breaks *in vitro*. Employing two doses of Zeocin in an iron-metal catalysed reaction that mimics the activation of Zeocin in cellular conditions[42], we introduced SSBs (0.05 mg/mL Zeocin; producing nicked-circular DNA) and a mixture of DSBs and DSBs (0.5 mg/mL Zeocin; producing nicked-circular DNA and linear DNA forms) into plasmid DNA. SNM1A was capable of extensively digesting all forms of the nicked and linear forms of DNA molecule (Fig.7B), consistent with a capacity to exonucleolytically process the existence chemical modifications induce by radiomimetics at the sites of the DNA breaks they induce.

Discussion

Disruption of SNM1A in human cells revealed a novel and unanticipated phenotype, namely a profound sensitivity to radiomimetic drugs as well as sensitivity to IR treatment. This is associated with delayed resolution of these breaks. Moreover, SNM1A is recruited to the complex DNA breaks induced by radiomimetics, IR and long-wave laser damage within minutes of damage induction. Multiple potential ligand-interacting motifs are present in the N-terminal region of SNM1A, proximal to the MBL-β-CASP domain which forms the catalytic core of the enzyme and active site[15]. Systematic examination of the role of the putative interaction and recruitment motifs revealed an important role for the PIP box and PBZ motif in the efficient initial recruitment of SNM1A to sites of complex breaks. This implies that interaction with PCNA (which is itself very rapidly recruited to laser-induced damage, as demonstrated here and by others) and PAR chains is critical to for the timely recruitment of SNM1A to laser damage. This is consistent with the previously documented PIP box-mediated interaction of SNM1A with PCNA[18], and data presented here demonstrates that SNM1A interacts with PAR-chains *in vitro*, in a PBZ-dependent manner. Moreover, trapping and inhibiting poly-ADP-ribose polymerase (PARP) with the inhibitor Olaparib phenocopies mutation of the PBZ motif, delaying SNM1A recruitment to laser damage. Indeed, co-

disruption of the PIP box with the PBZ completely abrogates the recruitment of SNM1A to the sites of laser and Zeocin-induced breaks and, consistently, so does mutation of the PIP box when combined with Olaparib treatment. SNM1A also contains a UBZ motif, adjacent to its PBZ. Like the PIP box of SNM1A, the UBZ has previously been demonstrated to be important for the recruitment or retention of SNM1A to the sites of ICL damage during S-phase. In response to laser-induced damage, mutation of the UBZ produced a phenotype distinct from that observed by mutation of the UBZ or PIP. Importantly, this suggests that the mutations introduced into the neighbouring UBZ or PBZ do not mutually impact on the function of the other motif. UBZ mutant SNM1A is recruited with normal initial kinetics to laser damage but fails to accumulate to the same level. A screen of ubiquitin E3 ligases that are known to deposit ubiquitin at sites of DNA breaks, which are therefore candidates for providing the ligand for the interaction with the SNM1A UBZ motif, revealed that Rad18 loss phenocopies mutation of the UBZ, leading to reduced overall levels of accumulation of SNM1A at laser stripes. PCNA (lysine 164) remains the only known target for Rad18 ubiquitination[43], but we were unable to defect PCNA ubiquitination following IR or Zeocin treatment, either in whole cell extracts or by performing immunoprecipitations with an antibody directed against monoubiquitinated PCNA. It is likely that the fraction of PCNA that is modified is very small, but we were unable to definitively address this point.

The phenotype of cell disrupted for homologues of SNM1A have been examined in multiple organisms, from yeast to human, and have confirmed an evolutionarily conserved role in the repair of ICLs. However, where the sensitivity and a response to IR and radiomimetics has been examined in vertebrate cells, only human cells have been implicated in response to these forms of damage. In the case of mouse ES cells and chicken DT-40 cells no marked sensitisation to IR was observed[44-46]. However, work from Richie and colleagues noted that human SNM1A forms subnuclear foci following IR treatment[47], and that these foci co-localise with 53BP1 and Mre11, providing early evidence for a role for SNM1A in the repair of radiation-induced DSBs. A potential explanation for these interspecies differences rest with the fact that vertebrates harbour three SNM1 paralogues, SNM1A, SNM1B/Apollo and SNM1C/Artemis. Based upon significant similarities in their enzymatic activity, as 5'-3' exonucleases, SNM1B might plausibly play a related or redundant role in the processing of radiation-induced DSBs. Indeed, multiple reports indicate that loss of murine SNM1B is associated with cellular radiosensitivity. Therefore, in mice the roles of SNM1A and SNM1B in the repair of complex DNA breaks might only be revealed once such redundancy or species-specific prioritisation or their roles is systematically examined. Moreover, Artemis deficient cells are IR sensitive and Artemis plays a well-documented role in the removal of several end-blocking chemical modifications during the repair of complex breaks. Interestingly, disruption of the SNM1A homologue in budding yeast, Pso2 together with inactivation of the nuclease Mre11 (*via* an *mre11-H125N* mutation) leads to a profound sensitivity to IR, suggesting that these two nucleases play redundant roles in processing complex DNA ends[48]. Notably, like *pso2* and *mre11* single mutants, *pso2 mre11-H125N* double mutant cells did not display any overt defects in the repair of 'clean DSBs' induced by the HO-endonuclease, analogous to the situation we report here for SNM1A in the I-Sce-1 reporter assay. This suggests that the key function of Pso2 and SNM1A (and a known major function of Mre11 of the nuclease activity) is in the processing of chemical modification of the DNA at 'dirty' break termini prior to their repair, rather than direct participation in the DSB process *per se*. Mre11 is also implicated in the initiation of DSB resection and repair cells by clearing covalently linked proteins at break

termini, for example the DNA-topoisomerase 1 (Top1) crosslinks induced through Camptothecin (CPT) treatment[49,50]. However, we see no role evidence for SNM1A in this process, based on the wild-type like sensitivity of SNM1A cells to CPT. Moreover, it is interesting to note that co-inactivation of Pso2 with Exo1, the only other known major 5′-3′ repair exonuclease in yeast, does not strongly impact on IR sensitivity[48]. This implies that Exo1 is not a major factor acting to process ends in the absence of Pso2, and *vice versa*. Our finding that the exonuclease activity of human Exo1, a close functional relative of yeast Exo1, is highly sensitivity to the presence of chemical lesions is consistent with this. It seems likely that both Mre11 (through its 3′-5′ exonuclease or endonuclease activities) and SNM1A (through its 5′-3′ exonuclease activity) are well equipped to deal with a set of the chemical lesions induced at break termini by radiation and play a major role in this important defence against complex DSBs.

Therefore, a careful and comprehensive examination of the relationship between all three SNM1 paralogues in mammalian cells, in addition to their contribution relative other established and putative end-processing nucleases, is warranted in future studies.

Acknowledgements
This work was supported by a Cancer Research UK Programme Award (CRUK/ A24759) to PJM and CJS. MR is in receipt of an MRC Graduate Studentship and SL was supported by a National Science Scholarship from the Singaporean Agency for Science, Technology, and Research (A*STAR). We thank Lucy Henderson and Abimael Cruz-Migoni for help producing peptides, and Opher Gileadi for purified APLF.

References

1 Scully, R., Panday, A., Elango, R. & Willis, N. A. DNA double-strand break repair-pathway choice in somatic mammalian cells. *Nat Rev Mol Cell Biol* **20**, 698-714, doi:10.1038/s41580-019-0152-0 (2019).

2 Chapman, J. R., Taylor, M. R. & Boulton, S. J. Playing the end game: DNA double-strand break repair pathway choice. *Mol Cell* **47**, 497-510, doi:10.1016/j.molcel.2012.07.029 (2012).

3 Shibata, A. & Jeggo, P. A historical reflection on our understanding of radiation-induced DNA double strand break repair in somatic mammalian cells; interfacing the past with the present. *Int J Radiat Biol* **95**, 945-956, doi:10.1080/09553002.2018.1564083 (2019).

4 Kieffer, S. R. & Lowndes, N. F. Immediate-Early, Early, and Late Responses to DNA Double Stranded Breaks. *Front Genet* **13**, 793884, doi:10.3389/fgene.2022.793884 (2022).

5 Zhou, T. *et al.* Deficiency in 3'-phosphoglycolate processing in human cells with a hereditary mutation in tyrosyl-DNA phosphodiesterase (TDP1). *Nucleic Acids Res* **33**, 289-297, doi:10.1093/nar/gki170 (2005).

6 Chappell, C., Hanakahi, L. A., Karimi-Busheri, F., Weinfeld, M. & West, S. C. Involvement of human polynucleotide kinase in double-strand break repair by non-homologous end joining. *EMBO J* **21**, 2827-2832, doi:10.1093/emboj/21.11.2827 (2002).

7 Rass, U., Ahel, I. & West, S. C. Actions of aprataxin in multiple DNA repair pathways. *J Biol Chem* **282**, 9469-9474, doi:10.1074/jbc.M611489200 (2007).

8 Takahashi, T. *et al.* Aprataxin, causative gene product for EAOH/AOA1, repairs DNA single-strand breaks with damaged 3'-phosphate and 3'-phosphoglycolate ends. *Nucleic Acids Res* **35**, 3797-3809, doi:10.1093/nar/gkm158 (2007).
9 Gueven, N. *et al.* Aprataxin, a novel protein that protects against genotoxic stress. *Hum Mol Genet* **13**, 1081-1093, doi:10.1093/hmg/ddh122 (2004).
10 Iles, N., Rulten, S., El-Khamisy, S. F. & Caldecott, K. W. APLF (C2orf13) is a novel human protein involved in the cellular response to chromosomal DNA strand breaks. *Mol Cell Biol* **27**, 3793-3803, doi:10.1128/MCB.02269-06 (2007).
11 Moshous, D. *et al.* Artemis, a novel DNA double-strand break repair/V(D)J recombination protein, is mutated in human severe combined immune deficiency. *Cell* **105**, 177-186, doi:10.1016/s0092-8674(01)00309-9 (2001).
12 Ma, Y., Pannicke, U., Schwarz, K. & Lieber, M. R. Hairpin opening and overhang processing by an Artemis/DNA-dependent protein kinase complex in nonhomologous end joining and V(D)J recombination. *Cell* **108**, 781-794, doi:10.1016/s0092-8674(02)00671-2 (2002).
13 Inamdar, K. V. *et al.* Conversion of phosphoglycolate to phosphate termini on 3' overhangs of DNA double strand breaks by the human tyrosyl-DNA phosphodiesterase hTdp1. *J Biol Chem* **277**, 27162-27168, doi:10.1074/jbc.M204688200 (2002).
14 Ahel, I. *et al.* The neurodegenerative disease protein aprataxin resolves abortive DNA ligation intermediates. *Nature* **443**, 713-716, doi:10.1038/nature05164 (2006).
15 Baddock, H. T. *et al.* The SNM1A DNA repair nuclease. *DNA Repair (Amst)* **95**, 102941, doi:10.1016/j.dnarep.2020.102941 (2020).
16 Pettinati, I., Brem, J., Lee, S. Y., McHugh, P. J. & Schofield, C. J. The Chemical Biology of Human Metallo-beta-Lactamase Fold Proteins. *Trends Biochem Sci* **41**, 338-355, doi:10.1016/j.tibs.2015.12.007 (2016).
17 Wang, A. T. *et al.* Human SNM1A and XPF-ERCC1 collaborate to initiate DNA interstrand cross-link repair. *Genes Dev* **25**, 1859-1870, doi:10.1101/gad.15699211 (2011).
18 Yang, K., Moldovan, G. L. & D'Andrea, A. D. RAD18-dependent recruitment of SNM1A to DNA repair complexes by a ubiquitin-binding zinc finger. *J Biol Chem* **285**, 19085-19091, doi:10.1074/jbc.M109.100032 (2010).
19 Schmiester, M. & Demuth, I. SNM1B/Apollo in the DNA damage response and telomere maintenance. *Oncotarget* **8**, 48398-48409, doi:10.18632/oncotarget.16864 (2017).
20 Baddock, H. T. *et al.* A phosphate binding pocket is a key determinant of exo- versus endo-nucleolytic activity in the SNM1 nuclease family. *Nucleic Acids Res* **49**, 9294-9309, doi:10.1093/nar/gkab692 (2021).
21 Pannicke, U. *et al.* Functional and biochemical dissection of the structure-specific nuclease ARTEMIS. *EMBO J* **23**, 1987-1997, doi:10.1038/sj.emboj.7600206 (2004).
22 Porteus, M. Design and testing of zinc finger nucleases for use in mammalian cells. *Methods Mol Biol* **435**, 47-61, doi:10.1007/978-1-59745-232-8_4 (2008).
23 Doudna, J. A. & Charpentier, E. Genome editing. The new frontier of genome engineering with CRISPR-Cas9. *Science* **346**, 1258096, doi:10.1126/science.1258096 (2014).

24 Povirk, L. F. DNA damage and mutagenesis by radiomimetic DNA-cleaving agents: bleomycin, neocarzinostatin and other enediynes. *Mutat Res* **355**, 71-89, doi:10.1016/0027-5107(96)00023-1 (1996).
25 Scully, R. & Xie, A. Double strand break repair functions of histone H2AX. *Mutat Res* **750**, 5-14, doi:10.1016/j.mrfmmm.2013.07.007 (2013).
26 Zimmermann, M. & de Lange, T. 53BP1: pro choice in DNA repair. *Trends Cell Biol* **24**, 108-117, doi:10.1016/j.tcb.2013.09.003 (2014).
27 Hopfner, K. P., Putnam, C. D. & Tainer, J. A. DNA double-strand break repair from head to tail. *Curr Opin Struct Biol* **12**, 115-122, doi:10.1016/s0959-440x(02)00297-x (2002).
28 Jasin, M. Homologous repair of DNA damage and tumorigenesis: the BRCA connection. *Oncogene* **21**, 8981-8993, doi:10.1038/sj.onc.1206176 (2002).
29 Ahel, I. *et al.* Poly(ADP-ribose)-binding zinc finger motifs in DNA repair/checkpoint proteins. *Nature* **451**, 81-85, doi:10.1038/nature06420 (2008).
30 Hurley, J. H., Lee, S. & Prag, G. Ubiquitin-binding domains. *Biochem J* **399**, 361-372, doi:10.1042/BJ20061138 (2006).
31 De Biasio, A. & Blanco, F. J. Proliferating cell nuclear antigen structure and interactions: too many partners for one dancer? *Adv Protein Chem Struct Biol* **91**, 1-36, doi:10.1016/B978-0-12-411637-5.00001-9 (2013).
32 Rizzo, A. A., Salerno, P. E., Bezsonova, I. & Korzhnev, D. M. NMR structure of the human Rad18 zinc finger in complex with ubiquitin defines a class of UBZ domains in proteins linked to the DNA damage response. *Biochemistry* **53**, 5895-5906, doi:10.1021/bi500823h (2014).
33 Eustermann, S. *et al.* Solution structures of the two PBZ domains from human APLF and their interaction with poly(ADP-ribose). *Nat Struct Mol Biol* **17**, 241-243, doi:10.1038/nsmb.1747 (2010).
34 Gulbis, J. M., Kelman, Z., Hurwitz, J., O'Donnell, M. & Kuriyan, J. Structure of the C-terminal region of p21(WAF1/CIP1) complexed with human PCNA. *Cell* **87**, 297-306, doi:10.1016/s0092-8674(00)81347-1 (1996).
35 Botchway, S. W., Reynolds, P., Parker, A. W. & O'Neill, P. Laser-induced radiation microbeam technology and simultaneous real-time fluorescence imaging in live cells. *Methods Enzymol* **504**, 3-28, doi:10.1016/B978-0-12-391857-4.00001-X (2012).
36 Traenkle, B. & Rothbauer, U. Under the Microscope: Single-Domain Antibodies for Live-Cell Imaging and Super-Resolution Microscopy. *Front Immunol* **8**, 1030, doi:10.3389/fimmu.2017.01030 (2017).
37 Ulrich, H. D. Regulating post-translational modifications of the eukaryotic replication clamp PCNA. *DNA Repair (Amst)* **8**, 461-469, doi:10.1016/j.dnarep.2009.01.006 (2009).
38 Lee, D. H. & Goldberg, A. L. Proteasome inhibitors: valuable new tools for cell biologists. *Trends Cell Biol* **8**, 397-403, doi:10.1016/s0962-8924(98)01346-4 (1998).
39 D'Andrea, A. D. Mechanisms of PARP inhibitor sensitivity and resistance. *DNA Repair (Amst)* **71**, 172-176, doi:10.1016/j.dnarep.2018.08.021 (2018).
40 Sengerova, B. *et al.* Characterization of the human SNM1A and SNM1B/Apollo DNA repair exonucleases. *J Biol Chem* **287**, 26254-26267, doi:10.1074/jbc.M112.367243 (2012).

41 Cadet, J., Douki, T., Gasparutto, D. & Ravanat, J. L. Oxidative damage to DNA: formation, measurement and biochemical features. *Mutat Res* **531**, 5-23, doi:10.1016/j.mrfmmm.2003.09.001 (2003).
42 Chen, J. & Stubbe, J. Bleomycins: towards better therapeutics. *Nat Rev Cancer* **5**, 102-112, doi:10.1038/nrc1547 (2005).
43 Fan, L., Bi, T., Wang, L. & Xiao, W. DNA-damage tolerance through PCNA ubiquitination and sumoylation. *Biochem J* **477**, 2655-2677, doi:10.1042/BCJ20190579 (2020).
44 Dronkert, M. L. *et al.* Disruption of mouse SNM1 causes increased sensitivity to the DNA interstrand cross-linking agent mitomycin C. *Mol Cell Biol* **20**, 4553-4561, doi:10.1128/MCB.20.13.4553-4561.2000 (2000).
45 Ahkter, S. *et al.* Snm1-deficient mice exhibit accelerated tumorigenesis and susceptibility to infection. *Mol Cell Biol* **25**, 10071-10078, doi:10.1128/MCB.25.22.10071-10078.2005 (2005).
46 Ishiai, M. *et al.* DNA cross-link repair protein SNM1A interacts with PIAS1 in nuclear focus formation. *Mol Cell Biol* **24**, 10733-10741, doi:10.1128/MCB.24.24.10733-10741.2004 (2004).
47 Richie, C. T. *et al.* hSnm1 colocalizes and physically associates with 53BP1 before and after DNA damage. *Mol Cell Biol* **22**, 8635-8647, doi:10.1128/MCB.22.24.8635-8647.2002 (2002).
48 Lam, A. F., Krogh, B. O. & Symington, L. S. Unique and overlapping functions of the Exo1, Mre11 and Pso2 nucleases in DNA repair. *DNA Repair (Amst)* **7**, 655-662, doi:10.1016/j.dnarep.2007.12.014 (2008).
49 Sacho, E. J. & Maizels, N. DNA repair factor MRE11/RAD50 cleaves 3'-phosphotyrosyl bonds and resects DNA to repair damage caused by topoisomerase 1 poisons. *J Biol Chem* **286**, 44945-44951, doi:10.1074/jbc.M111.299347 (2011).
50 Hartsuiker, E., Neale, M. J. & Carr, A. M. Distinct requirements for the Rad32(Mre11) nuclease and Ctp1(CtIP) in the removal of covalently bound topoisomerase I and II from DNA. *Mol Cell* **33**, 117-123, doi:10.1016/j.molcel.2008.11.021 (2009).
51 Mirdita, M. *et al.* ColabFold: making protein folding accessible to all. *Nat Methods* **19**, 679-682, doi:10.1038/s41592-022-01488-1 (2022).
52 Pettersen, E. F. *et al.* UCSF ChimeraX: Structure visualization for researchers, educators, and developers. *Protein Sci* **30**, 70-82, doi:10.1002/pro.3943 (2021).
53 Pastwa, E., Neumann, R. D. & Winters, T. A. In vitro repair of complex unligatable oxidatively induced DNA double-strand breaks by human cell extracts. *Nucleic Acids Res* **29**, E78, doi:10.1093/nar/29.16.e78 (2001).
54 Pierce, A. J., Johnson, R. D., Thompson, L. H. & Jasin, M. XRCC3 promotes homology-directed repair of DNA damage in mammalian cells. *Genes Dev* **13**, 2633-2638, doi:10.1101/gad.13.20.2633 (1999).
55 Bennardo, N., Cheng, A., Huang, N. & Stark, J. M. Alternative-NHEJ is a mechanistically distinct pathway of mammalian chromosome break repair. *PLoS Genet* **4**, e1000110, doi:10.1371/journal.pgen.1000110 (2008).

Materials and Methods

Cell lines

Cell lines U2OS and 293FT were cultured as per ATCC guidelines.

Creation of SNM1A$^-$ cell lines using genome engineering

Zinc Finger nucleases (ZFN) and CRISPR-Cas9 genome editing technologies were employed to make stable deletion-disruptions in DCLRE1A, the gene encoding SNM1A.

CompoZr ZFNs were designed by and purchased through Sigma-Aldrich with a detection and cut site in the DCLRE1A gene as follows (cut site in lowercase):
TGCCAGATGCCTTTTtcctcATTGATAGGGCAGAC

Cells were transfected with 1.3 µg of each of the plasmids containing the forward and reverse ZFNs in 10 µL of lipofectamine 2000 in a total volume of 200 µL OptiMEM media (Sigma). The transfection mix was incubated for 10 minutes to allow the complexes to form before being added to 5 x 10^5 cells that were freshly plated in a volume of 2 mL in wells of a 6-well plate. Media was changed 12-18 hours later and following a further 72 hours cells were analysed for genomic insertions or deletions using the SURVEYOR Mutation Detection Assay (Integrated DNA Technologies, Cel I assay). Once a pooled cell population was identified to contain cells with altered genomes, dilution cloning was performed. Clones, once grown, were then assayed for alterations to their genome through genomic PCR. Identified SNM1A$^-$ clones were further validated by analysing SNM1A protein levels (through SDS-PAGE/Western blot techniques) and mRNA levels (through QRT-PCR).

CRISPR-Cas9 genome editing was performed using sgRNAs designed using an inhouse design tool. The genomic target for the CRISPR-Cas9 sgRNAs of the DCLRE1A gene were as follows:

(1) **TCATAAACTGGACGTATCTTTGG** [posn: 334 - 356, -ve]

target genomic coordinates	strand	genome seq	RefSeq transcript
chr10:115612586-115612608	+ve	TCATAAACTGGACGTATCTTTGG	NM_001271816, NM_014881

(2) **ACATTTCCGAAGAAGACATTTGG** [posn: 11 - 33, +ve]

target genomic coordinates	strand	genome seq	RefSeq transcript
chr10:115612909-115612931	-ve	ACATTTCCGAAGAAGACATTTGG	NM_001271816, NM_014881

These cuts remove the majority of exon 1 of the DCLRE1A gene. The sgRNAs were cloned in to CRISPR-Cas9 vectors pX330 and pX458 carrying GFP and RFP fluorescence expression markers respectively.

Once treated with both plasmids (as above for ZFNs) cells were sorted by FACS to collect individual GFP and RFP positive cells in a well of a 96 well plate. These clones were allowed to grow (as above) before being analysed for genomic alterations (as above).bSNM1A$^-$ cells used for this study are detailed in Suppl Figure 1.

Cell transfections for protein expression

Transfection of a plasmids containing wild type SNM1A protein and mutations in the domains of interest as listed in Table 1. Cells (5 x 10^5) were transfected with 2.6 µg plasmid in 2 mL media with lipofectamine 2000 (ThermoFisher scientific) following manufacturer's recommendations in 35 mm glass bottom "µ-Dish" dishes (Ibidi) for laser microirradiation or analysis of drug induced DNA damage (foci). The transient expression of SNM1A-GFP (wild type and mutant) plasmids was performed with 2.6 µg of plasmid transfected with lipofectamine 2000 as above.

Table 1: mutations introduced into pEGFP-C1-SNM1A

Domain	Mutation(ref)
Nuclease domain inactivating substitution	D736A
Ubiquitin-binding zinc finger (UBZ)	C125F
Ubiquitin-binding zinc finger PBZ	C155A, C161A
PCNA-interacting motif (PIP box)	Y562A, F563A

For creation of cells stably expressing plasmids containing eGFP-SNM1A or a chromobody (Chromotek) of RFP-PCNA 5 x 10^5 cells were seeded and immediately transfected with the desired plasmid (2.6 µg) with a reduced amount of lipofectamine 2000 (2 µL) in a total volume of 200 µL. The reduced volume of lipofectamine 2000 was determined to reduce the toxicity of the transfection process. Complexes were allowed to form for 10 minutes and then added dropwise to the cells. After 3 hours, the media was changed and the cells allowed to grow for 24 hours. At this stage, the cells were sorted and single cells expressing the fluorescence marker associated with the plasmid were plated out in a 96 well plate and allowed to grow until 50-75% confluent. Cells were transferred to 25 cm^2 flasks and allowed to grow further. Once 60-80% confluent, cells were analysed for fluorescence and clones that exhibited adequate level of fluorescence were further analysed by microscopy-based techniques and SDS-PAGE and western blot protocols to establish the expected phenotype of the created clone.

Cells that had successfully integrated the pEGFP-C1 plasmid into their genome were first selected with Kanamycin before being sorted by FACS into single wells in a 96 well plate, and grown up as a clonal population.

BRCA2 siRNA Transfections

Cells were treated with 20 nM siRNA against BRCA2 (GGGAAACACUCAGAUUAAAUUdTdT and AAUUUAAUCUGAGUGUUUCCCdTdT, Life Technologies) in HiPerFect transfection reagent (Qiagen) using a fast-forward transfection protocol then further siRNA is added 24 hours later.

Cell treatments with DNA damaging drugs and radiation

Cell treatments were as followed unless otherwise stated in figure legends. Cisplatin (CDDP, Teva pharmaceutical industries Ltd., Eastbourne, UK. Cat # 51642169) was the formulated drug, concentrate for infusion, including 1mg/mL cisplatin with sodium chloride, hydrochloric acid/sodium hydroxide (for pH adjustment). If required, CDDP was diluted in PBS. Zeocin (Invitrogen, Thermo Fisher Scientific, Cat # R25001) was diluted in PBS. Treatments were at 0.1mg/mL for 2h unless otherwise listed in figure legends. Ionising radiation induced damage

(IR) was induced using caesium 137 source. SJG-136 (a kind gift from John Hartley, UCL) was dissolved in H_2O and treatments were performed continuously. Olaparib was made up in PBS and clonogenic treatments were continuous. Formaldehyde (16%, methanol free, Taab Laboratories Equipment) was always freshly diluted in PBS and used immediately. UVC treatments were performed in a Stratagene, UV stratalinker 2400 with UV-C lamps. Media was removed from the dishes, the cells were dosed and fresh media replaced. Hydrogen peroxide was diluted in PBS from a stock 30% solution (BDH, Cat#BDH7741-1). MG-132 (Med Chem Express) was dissolved in DMSO and cells were treated with 5 µM.

Colony counting/clonogenic assays

Clonogenic assays were performed in 10 cm tissue culture dishes (for U2OS and clones) or T75cm^2 tissue culture flasks (293FT cells, due to their reduced colony forming ability). Cells being 1000 per dish for U2OS and 2000 per flask for 293FT were seeded in complete media (10 mL and 20 mL respectively) and allowed to attach overnight before being treated with desired agents. Following treatments (short or continuous) cells were allowed to grow and form colonies for 10 days. Colonies formed were stained with coomassie R250 (Sigma) and counted on a COLCount Colony Counter (Oxford Optronix). All experiments represent the mean (±SEM) of at least three biological repeats of duplicate dishes/flasks for each treatment.

Structure prediction

ColabFold Google Colabs notebooks were used to predict the structures of the UBZ, PBZ and PIP Box (https://colab.research.google.com/github/sokrypton/ColabFold/blob/main/AlphaFold2.ipynb)[51]. with default parameters and inputting the sequences as follows (numbering as for human SNM1A; NCBI /NP_001258745.1/): UBZ = 112-148; PBZ =153-182; and PIP = 552-573. Coordinates of the highest-ranking AlphaFold models were then visualised, aligned to prior structures, and rendered using ChimeraX[52]. Alignments were made to prior structures as follows: RAD18 UBZ - PDB 2MRF[32]; APLF PBZ - PDB 2KQB[33]; PCNA with P21 PIP - PDB 1AXC[34].

DNA content and cell cycle FACS analysis

An estimation of distribution of cell cycle phase of treated cells was performed using BrdU incorporation and DNA content analysis as previously described[17].

Laser damage striping

DNA damage microscopy experiments were conducted on both a Zeiss 780 and a Zeiss 880 inverted confocal using a Plan-APO 63X 1.40NA oil immersion objective, with the optical zoom adjusted to a projected pixel size of 100 nm, at physiological conditions (37°C and 5% CO2). Prior to all experiments, care was taken to adjust the collimation of the 405 nm laser such that the z-focus aligned with the visible lasers (488, 561, and 633 nm) as determined by imaging of 200 nm diameter TetraSpeck beads. The laser power of the 405 nm lasers on both the Zeiss 780 and the Zeiss 880, as measured at the focal plane of a 10X 0.45NA air objective, was about 5 mW.

In these experiments, we induced a DNA damage sites by defining a rectangular ROI damage site within the cell nuclei with varied length (6.5 µm for single cell experiments and around 200 µm for multi-cell experiments) but fixed width of 1 µm. The laser damage was then done by using the 405 nm at full laser power, a scan speed pixel dwell time setting of 8 µs, and with

25 line iterations. In order to observe recruitment of EGFP tagged wild-type and mutant SNM1A to the DNA damage sites, we subsequently performed time-lapse experiments for a total of 80 image frames at a frame interval of 15 sec where the 405 nm laser induced DNA damage was initiated after image frame 5. EGFP emission in these experiments were collected on GaAsP detector, with a pinhole setting of 1 AU, a bandpass emission setting of 499-544 nm, a pixel dwell time of 1.58 µs, and with a line averaging setting of 4.

Quantitative analysis of the active recruitment to the DNA damage site was performed by use of Image J and Mathematica. In this analysis, we extracted the mean fluorescence intensity F(t)Bleach from a region-of-interest (ROI), superimposed on the DNA damage site, relative to the mean fluorescence intensity at a site on the same cell but away from the damage site F(t)Control) as a function of time, from several cells. The data was further normalized by the fluorescence intensity F(-) prior to the induction of the DNA damage such that active recruitment results in a ratio of [F(t)/F(-)]Bleach / [F(t)/F(-)]Control > 1 versus no recruitment or passive recruitment results in a ratio of [F(t)/F(-)]Bleach / [F(t)/F(-)]Control <= 1. The presented normalized data represents the mean (+/- SEM) for at least N=10 cells.

Cells were scanned in a variety of phases of the cell cycle. We determined the cell cycle phase using multiple approaches. The PCNA forms foci during DNA replication, which indicates the cells are in S-Phase. Morphology indicates G1 (about to undergo DNA synthesis) and G2 (about to undergo mitosis) as has been previously described

Table of antibodies

Shown in Table 2, below:

Table 2 - Antibodies used for western analysis and microscopy

Antibody	Supplier	Catalogue Number	Species	Clonality	Dilution used[1]
Glutathione-S-Transferase (GST)	Merck	G1160	Mouse	Mono	1:1000
APLF	Abcam	AB105446	Rabbit	Poly	1:1000
Anti-poly-ADP-ribose	Merck	MABE1031			
SNM1A	Bethyl Laboratories	A303-747A	Rabbit	Poly	1:1000
Ub PCNA (K164)	Cell Signalling	134395	Rabbit	Mono	1:1000
PCNA (Ms)	Santa Cruz	SC-056	Mouse	Mono	1 :1000
PCNA (Rb)	Abcam	AB92552	Rabbit	Mono	
BrdU	Abcam	AB6326	Rabbit	Mono	1:1000
β-Actin-HRP	Merck	A3854	Mouse	Mono	1:20,000
53BP1 (Ms)	Millipore	MAB3802	Mouse	Mono	
53BP1 (Rb)	Abcam	AB175933	Rabbit	Mono	
γH2AX (Ms)	Millipore	JBW301	Mouse	Mono	
γH2AX (Rb)	Abcam	Ab81299	Rabbit	Mono	

[1] Dilutions listed are for western blot protocols. All dilutions for microscopy work were at 1:200

Immunoblot (western) analysis

Was performed as previously described[17]. All secondary antibodies were raised in goat (Dako, Agilent technologies) and used at 1:5000 in TBT-T (Tris-buffered saline with 0.1% Tween).

Microscopic analysis of damage-induced subnuclear foci

To assess the number of nuclear foci following treatments, cells were plated in glass bottom dishes (as above) and allowed to attached. Following treatment, cells were fixed with 4% Formaldehyde in PBS, blocked with IF blocking buffer (5% Horse serum, 1% Saponin in PBS) for 1hr before being incubating with primary antibodies at desired concentrations in IF blocking buffer overnight at 4°C. After washing cells three times with PBS, cells were incubated with secondary antibodies for 2-4 hrs in IF blocking buffer, washed a further 3 times with PBS then stained with Hoechst 333258 (1µg/mL in PBS) for 30 minutes before a further three washes (all washes and incubations were performed at room temperature unless otherwise stated).

Confocal images were obtained with a Plan APO 63X 1.40NA oil immersion objective, a pinhole setting of 1 AU, bandpass emission settings of 410-468 nm for Hoechst, 490-544 nm for EGFP, 579-624 nm for RFP or Alexa 568, and 633-695 nm for Alexa 647, a projected pixel dimension of around 110 nm x 110 nm, a pixel dwell time of 1.35 µs, and with a line averaging setting of 2. In order to ensure sufficient cell numbers (N>300), images were acquired in a tiled 5 x 5 format corresponding to an image are of about 0.65 mm x 0.65 mm. Images were imported into ImageJ and foci were counted using a macros adjusting for staining levels between experiments.

Isolation of GST- SNM1A peptides

To establish the role of binding of SNM1A and mutants with PAR chains, PCNA and ubiquitinated PCNA (UbPCNA) we generated GST-SNM1A peptide constructs. Consideration was given to the surrounding sequencing when designing these peptides a multiple sequence alignment was used to define the borders of the UBZ/PBZ domains and PIP box. Extra residues both upstream and downstream were included being 2+2 in the UBZ/PBZ peptide and 10+12 in the PIP box peptide. The peptide sequences were (variant amino acids in colour):

UBZ/PBZ Peptide

RPVYDGYCPNCQMPFSSLIGQTPRWHVFECLDSPPRSETECPDGLLCTSTIPFHYKRYTHFLLAQSRAG
The established mutations were introduced in to these peptides as previously described. The UBZ was mutated at C125F. The PBZ was mutated at C155A, C161A.

PIP Box

ARHPSTKVMKQMDIGVYFGLPPKRKEEKLL
Mutation Y562A, F563A.

GST alone control

GARLQAR

The sequence encoding these peptides were cloned into pET-41b using the restriction sites MfeI and SalI using standard methods and verified by sequencing.

The recombinant plasmid DNA for:

- GST blank
- Wildtype SNM1A (PU region)
- UBZ mutant (C125F)
- PBZ mutant (CC155,161AA)
- PBZ and UBZ mutant (C125F, C155A, C161A)
- Wildtype SNM1A (PIP Box)
- PIP mutant (Y562A,F563A)

Were transformed in to competent BL21 *E . coli* by heat-shock. Cultures (250 mL) were grown in 2 x YT media at 37°C until OD 0.6 was reached at which point incubation temperature was reduced to 16°C and protein expression was induced with IPTG (0.5 mM). Following 12-14 hour incubation cells were pelleted and snap frozen before being stored at -80°C.

PCNA and Ub-PCNA binding assay

GST-Peptides were isolated by resuspending a 50mL *E. coli* pellet in 7.5 mL of TBS-N (Tris buffered saline with 0.1% NP-40) and supplemented with 1 x protease inhibitor cocktail tables (Merck). Cells were sonicated for four rounds of one minute on, one minute off, on ice, to release the cellular contents before being centrifuged at 20,000 x g for 30 minutes at 4°C. Cleared lysates were added to pre-blocked glutathione-agarose beads (ThermoScientific, 400 µL of beads per sample, blocked with 5% FCS in PBSA for 1 hour) and binding was performed at 4°C for 2 hours. Peptide bound beads were washed with varied concentrations of PBS (salt at 250 mM, 500 mM, 1 M, 500 mM, 250 mM) before being resuspended in standard PBS. Samples were then divided and binding to PCNA or UbPCNA performed. Purified PCNA or UbPCNA (150 ng) was added to each sample and tumbled at 4°C for 1 hour. Washes were performed again as above to remove unbound PCNA/UbPCNA. The washed beads were resuspended in 2 x Laemelli buffer and boiled before being run on 4-12% SDS-PAGE gels and transferred to PVDF membrane for immunoblotting with anti-SNM1A, PCNA, UbPCNA and GST.

PAR Binding assay

To assess the binding of PAR (poly-ADP-ribose) chains to the ligand-binding motifs in SNM1A we utilised the GST-SNM1A PBZ/UBZ peptides described above. Native GST-SNM1A Peptides were extracted from the lysate of BL21 cells and the peptides were eluted off the beads with excess glutathione. These peptides were then dot-blotted to PVDF. The membrane containing the GST-SNM1A peptides as well as BSA and a known PAR interacting purified protein (APLF-1) as controls.

The membranes were blocked in 10% skimmed milk powder in PBS (10% milk) and a solution of Poly(ADP-ribose) polymers (1:1000 PAR chains in 10% milk, Trevigen) were incubated at room temperature for 1 hr to allow binding of the PAR chains to the proteins/peptides bound to the membrane. Following extensive washing (3 x 3 minutes) in TBS-T (Tris-buffered Saline with 0.1% Tween 20) the membranes were probed with an Anti-poly-ADP-ribose binding reagent (1:1000 in 10% milk, Merck) as well as anti-APLF and anti-GST as loading controls.

Nuclease assay; substrate preparation and assay conditions

Full-length SNM1A and its variants were purified as described[17]. Nuclease assays were performed as described[40]. Oligonucleotide substrates including those containing terminal and

internal 8-oxoGuanine lesions were purchased from Eurofins, MWG Operon, Germany. The sequences and features of the oligonucleotides used have been described in detail elsewhere[20].
Substrates were prepared as follows: 10 pmol of DNA oligonucleotide (Eurofins MWG Operon, Germany) were 3'-end labelled with 3.3 pmol of α-32P-dATP (Perkin Elmer) using terminal deoxynucleotidyl transferase (TdT, 20 U; ThermoFisher Scientific), incubated together at 37°C for 1 h. To remove unincorporated nucleotides, these were passed through a P6 Micro Bio-Spin chromatography column (BioRad). For the preparation of double-stranded substrates, radiolabelled single-strand oligos were annealed with the appropriate unlabelled oligonucleotides (1:1.5 molar ratio of labelled to unlabelled oligonucleotide) by heating to 95°C for 5 min, and then slowly cooling to room temperature in annealing buffer (10 mM Tris–HCl; pH 7.5, 100 mM NaCl, 0.1 mM EDTA).

Nuclease assays were performed in 10 µl volumes containing 20 mM HEPES-KOH, pH 7.5, 50 mM KCl, 10 mM MgCl2, 0.05% Triton X-100, 5% glycerol and 1 nM of SNM1B. Reactions were initiated by adding DNA substrate (10 or 100 nM), incubation was at 37°C for the indicated time period, and reactions terminated by adding 10 µl stop solution (95% formamide, 10 mM EDTA, 0.25% xylene cyanol, 0.25% bromophenol blue) and incubating at 95°C for 3 min.

Reaction products were analysed on 20% denaturing polyacrylamide gel electrophoresis (40% solution of 19:1 acrylamide:bis-acrylamide, BioRad) containing 7 M urea (Sigma Aldrich)) in 1× TBE (Tris-borate EDTA) buffer. Electrophoresis was at 700 V for 75 min. Gels were fixed for 40 min in a 50% methanol, 10% acetic acid solution, and vacuum-dried at 80°C for 2 h. Gels were imaged with using phosphorimager screen and scanned using a Typhoon 9500 phosphorimager (GE).

SNM1A processing of Zeocin induced DNA damage
To induce Zeocin damage in DNA plasmids (3.6 µg of pG46) were treated with Zeocin in 1 x reaction buffer[53] (12.5 mM Tris–HCl pH 8.0, 300 mM sucrose, 0.0188% Triton X-100, 1.25 mM EDTA, 5 mM $MgCl_2$ with freshly added 7.5 mM β-mercaptoethanol, 1% heat-inactivated BSA and 100 mM ferrous ammonium sulphate) in 50 µL volumes for 20 minutes at 37ºC. PCR clean-up columns (Qiagen) were used as per manufacturer's instructions to clean up the reacted plasmid DNA and eluted in a 50 µL volume in buffer EB (Qiagen).

The ability of SNM1A to digest Zeocin-induced damaged DNA was compared with Hind III linearised plasmid (an optimal substrate for SNM1A) by incubating the DNA substrates with varying concentrations of SNM1A for 1 hour at 37 ºC. Following digestion, the samples (3:1) were diluted in stop buffer (95 % v/v Formamide, 10 mM EDTA, 0.25% v/v Bromophenyl blue) and resolved in 1% agarose gels in 1 x TAE buffer.

Homologous Recombination Repair (HR) and Non-Homologous End Joining repair (EJ) reporter assays
HR and EJ repair assays were performed as previously described[54,55]

Plasmids pCMV-SceI and pDR-GFP (a kind gift from Valentine Macaulay) were used to measure HR and pimEJ5GFP (Addgene # 44026) and pCMV-SceI were used to measure EJ[55].

Plasmids (2.6 µg of each) were transfected into 5 x 10^5 cells (293FT, 293FT cells treated with siRNA to BRCA2, XRCC4$^-$ or SNM1A$^-$ 293FT cells) in 2 mL in wells of a 6-well plate, as described above. After 24 hrs cells were harvested and resuspended in fresh media containing no phenol red and analysed on an Attune flow cytometer (ThermoFisher Scientific) to assess GFP positive cells as a measure of repair in each pathway.

Figure legends.

Figure 1 *SNM1A$^-$ cells show a profound sensitivity to radiometric damage.* **A** SNM1A$^-$ cells generated in U2OS background are sensitive to Cisplatin (CDDP) treatment in a clonogenic survival assay and the sensitivity is suppressed in cells stably expressing an EGFP-SNM1A. Inset immunoblot: SNM1A protein is not detected in the SNM1A$^-$ cells (1A$^-$), compared to wildtype U2OS cells (U), and the EGFP-SNM1A band is evident in the complemented cell line (G) by immunoblot analysis as shown in the inset panels. **B.** SNM1A$^-$ cells are also sensitive to the DNA crosslinking agent SJG-136. **C.** SNM1$^-$ cells show a profound sensitivity to the radiomimetic Zeocin and this sensitivity is rescued by expressing EGFP-SNM1A. **E.** Zeocin sensitivity is also observed in a HEK293FT cells, and is also rescued with stable expression of EGFP-SNM1A. SNM1A protein is not detected in these cell lines by immunoblot analysis (panel **E** inset). **F. G. and H** Zeocin treatment induces persistent γH2AX and 53BP1 foci in SNM1A$^-$ cells indicating a failure to repair Zeocin/IR induced "dirty" DSB damage. (n=3 biological repeats counting >500 cells per repeat, error = SEM). Panel **J** shows representative foci images of the data from **F** and **G. I**. Cell cycle distribution by DNA content determined by flow cytometry following Zeocin treatment over 48 hours reveals a G2 accumulation in SNM1A$^-$ cells not observed WT U2OS cells.

Figure 2 *Formation of SNM1A and 53BP1 foci in response to Zeocin induced DNA damage.* **A.** EGFP-SNM1A and 53BP1 foci co-localise at sites of Zeocin-induced DNA damage. EGFP-SNM1A cells treated with Zeocin were fixed and stained with anti-53BP1. **B** High magnification of analysis of the co-localised EGFP-SNM1A and 53BP1 foci, deconvolved in Huygens Express.

Figure 3 *SNM1A contains conserved ubiquitin binding, PAR binding and PCNA interacting motifs.* **A** Schematic of domains and motifs of the SNM1A, including location of residues predicted to disrupt ligand binding for each motif (see panel B) *UBZ4* (ubiquitin-binding zinc-finger 4 – C125F), *PBZ* (PAR-binding zinc-finger – C155A/C161A), *PIP* (PCNA-interacting peptide – Y562A/F563A), and catalysis through the MBL/β-CASP (metallo-β-lactamase/CPSF-Artemis-SNM1-Pso2 – D736A). **B.** Structural alignment of these domains using AlphaFold predicted structures of the UBZ, PBZ and PIP box motifs of SNM1A against their respective equivalents from RAD18 (PDB 2MRF), APLF (PDB 2KQB) and P21 (PDB 1AXC). Highlighted amino acids reflect key conserved motifs which coordinate the Zn^{2+} for UBZ and PBZ, and fit into grooves within PCNA for the PIP box. **C.** GST-tagged peptides covering the PBZ, UBZ and and PIP box regions were generated (see Supplemental Figure 4) and used to pull-down PCNA and lysine-164 monoubiquitinated PCNA (UbPCNA). The wild-type PIP peptide binds and pulls down PCNA but not the PIP box mutant peptide (left hand panel), whereas the PIP box mutant does not. The wild-type peptide spanning the region containing the PBZ and UBZ motifs pulls down UbPCNA, but not PCNA, and a peptide containing mutated predicted PBZ and UBZ binding residues fails to pull down either PCNA or UbPCNA. **D.** Slot blot of analysis SNM1A-GST peptides blotted to PVDF membrane indicate only WT GST peptides spanning the PBZ

and UBZ motifs are able to bind PAR chains (top panel), whereas those harbouring predicted interaction-disrupting mutations in the PBZ or UBZ are not. The PAR binding protein APLF-1 is used as a control (bottom panel).

Figure 4 *Zeocin induces DNA damage that results in recruitment of SNM1A and 53BP1 to sites of damage*. **A** SNM1A, 53BP1 and γH2AX foci form and co-localise at sites of Zeocin DNA damage. These foci also form in the nuclease inactive D736A mutant (SNM1A^{NI}). **B** Mutations in the UBZ, PBZ and PIP motifs show an altered recruitment of EGFP-SNM1A to Zeocin-induced sites of DNA damage. **C.** Quantification of these damage response foci in **C**, displayed more than 3 repeats, error bars show the standard deviation.

Figure 5 *SNM1A is rapidly and readily recruited to laser-induced DNA damage.* **A.** EGFP-SNM1A is recruited to localised laser induced DNA damage (laser stripes) where it colocalises with 53BP1. Staining with Hoeschst 33258 was used to define nuclei. **B.** To analyse the recruitment of EGFP-SNM1A, stably expressing cells were monitored over 20 minutes and the fluorescence intensity at the sites of laser striping measured (see Material and Methods). Both wild-type EGFP-SNM1A (wt) and nuclease inactive EGFP-SNM1A^{NI} were recruited to laser damage with similar kinetics and intensity (quantified in panel **C**). **D.** Recruitment of EGFP-SNM1A was similar in G0/G1, S and G2-phases of the cell cycle (quantified in panel **E**). All laser striping experiments represent data from at least ten cells from three biological repeats, error bars are standard error of the mean.

Figure 6 *The UBZ, PBZ and PIP box motifs of SNM1A play a role in protein recruitment to sites of laser-induced DNA damage.* Panel **A** shows the motifs and residues mutated relevant to this figure. **B.** The recruitment of EGFP-SNM1A substitutions in the UBZ, PBZ and PIP box that ablate ligand-binging (see Fig. 3) were monitored following laser-induced damage, representative images shown in panel **C**. **D**. Double or triple co-substitution of key residues in the UBZ, PBZ and PIP box were used to investigate the cooperative contribution of these SNM1A motifs to laser stripe recruitment. **E**. Olaparib treatment reduces EGFP-SNM1A recruitment to laser stripes. **F.** The effect of combining PIP box mutation with Olaparib treatment on laser stripe recruitment. All laser striping experiments represent data from at least eight cells from three biological repeats, error bars are standard error of the mean.

Figure 7 *Purified SNM1A can digest complex DNA lesions* in vitro. **A.** Purified SNM1A Exo1, can digest 3′ radiolabelled dsDNA *in vitro.* SNM1A and Exo1 were also incubated with oligonucleotides with either an internal or a 5′-located 8-oxo-guanine (8-oxoG). SNM1A can digest past the altered 8-oxoG bases but Exo1 does not. **B.** Plasmid DNA (pG46) were treated with the restriction endonuclease HindIII (to linearise the DNA) or treated with Zeocin (to induced complex DNA breaks). Broken plasmids were treated with purified SNM1A and the resulting DNA products resolved on an agarose gel, stained with Ethidium bromide and visualised. SC = supercoiled DNA; ROC = Relaxed Open-Circular DNA; L = Linear DNA.

Swift, Figure 1

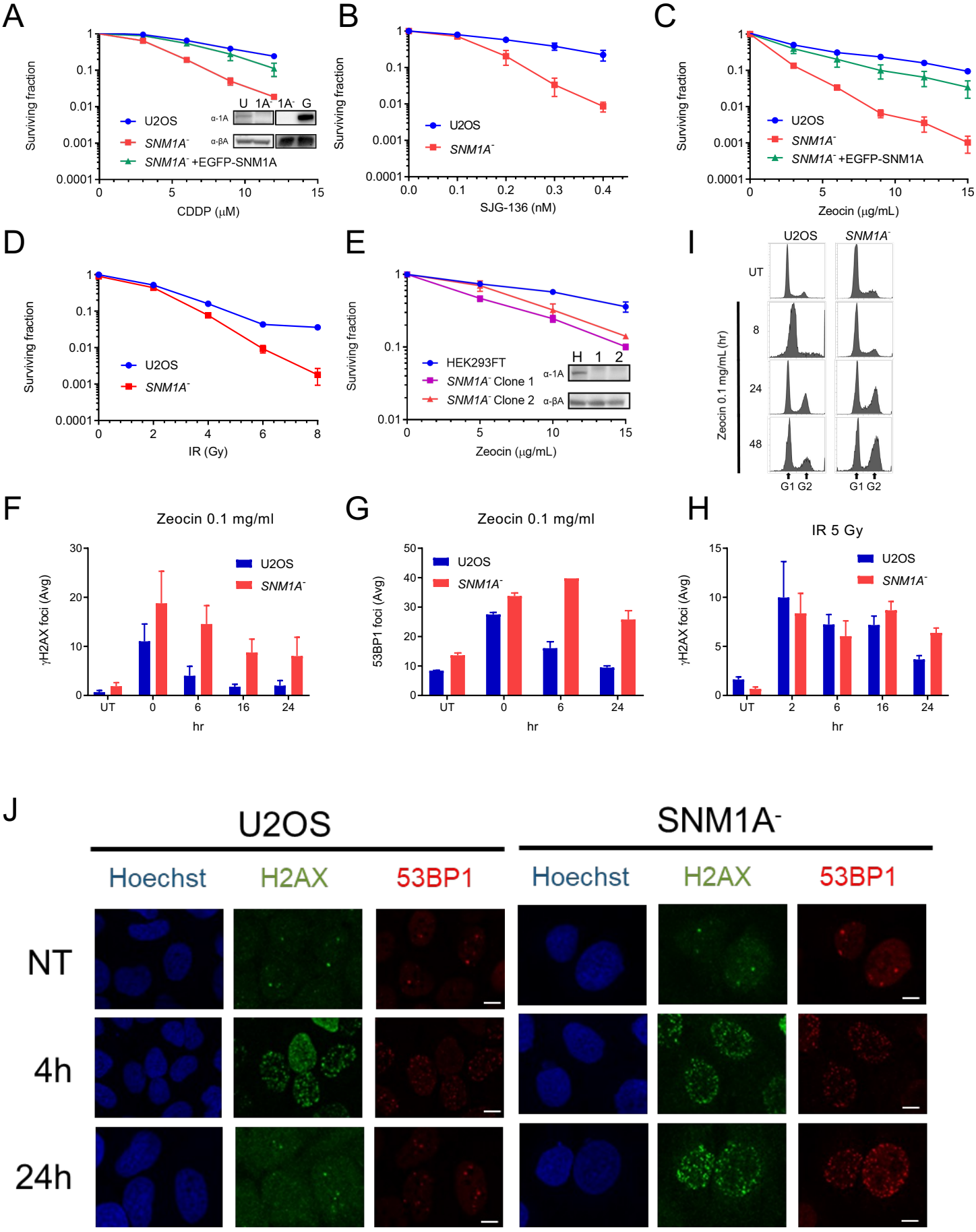

Swift, Figure 2

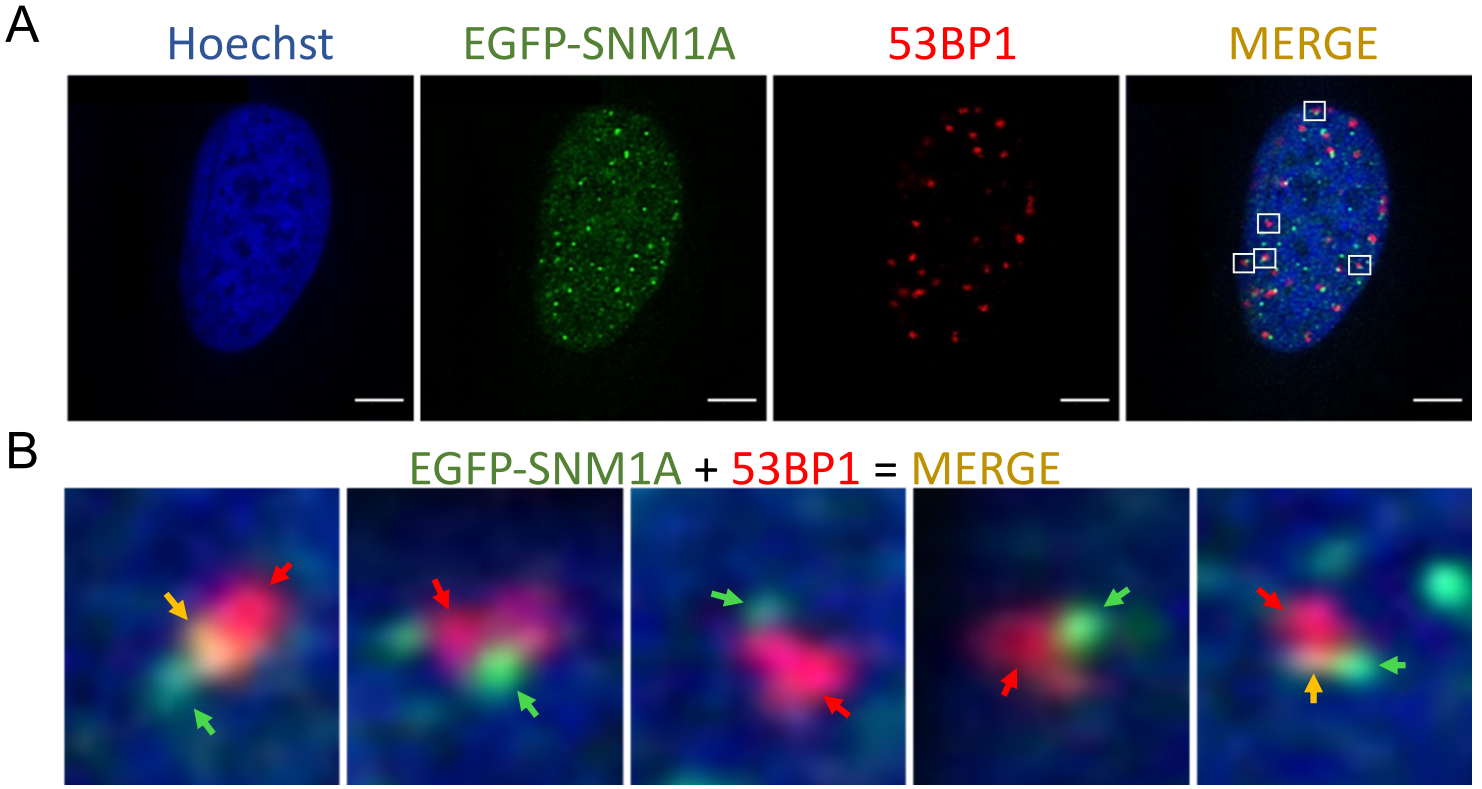

Swift, Figure 3

A

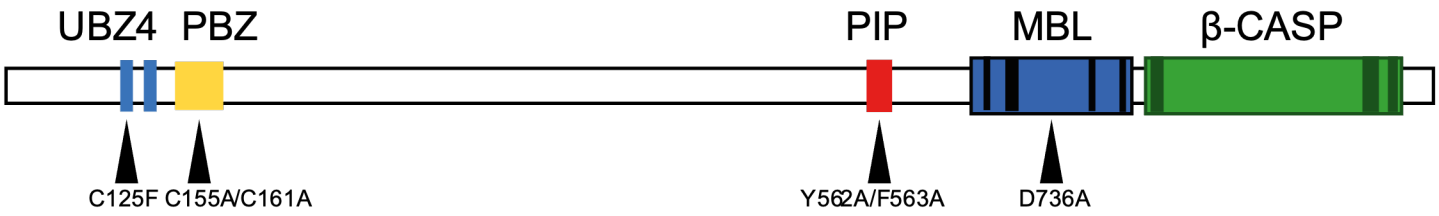

B

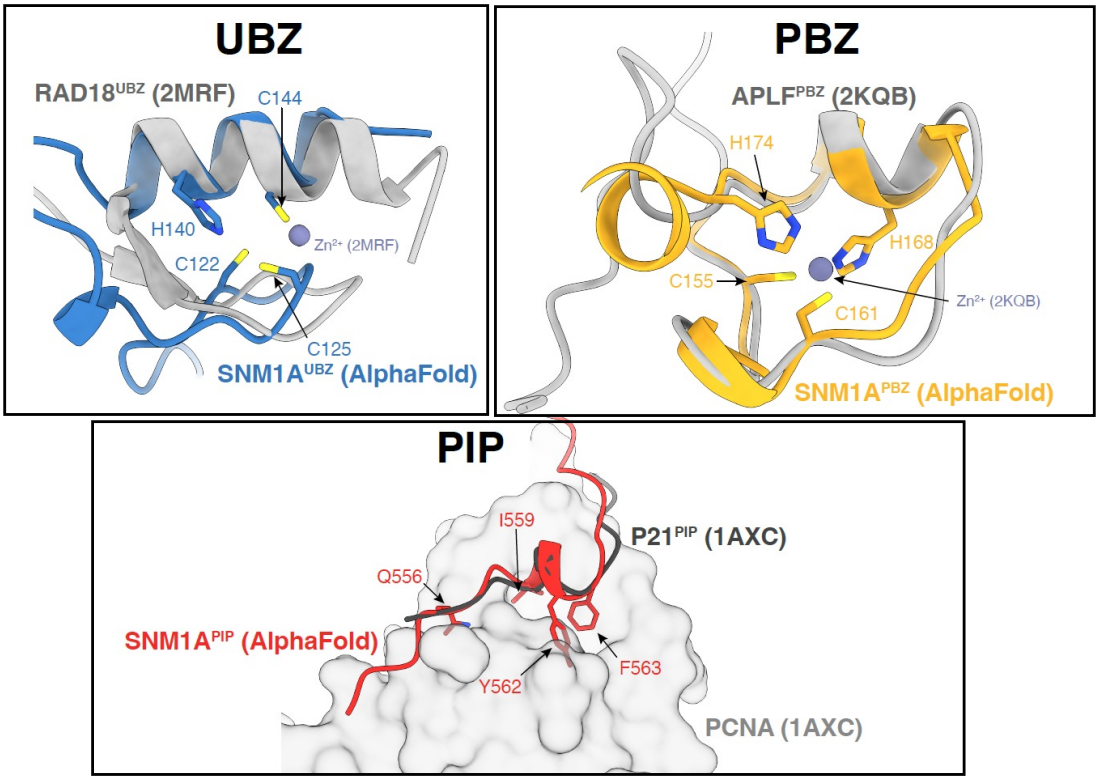

C

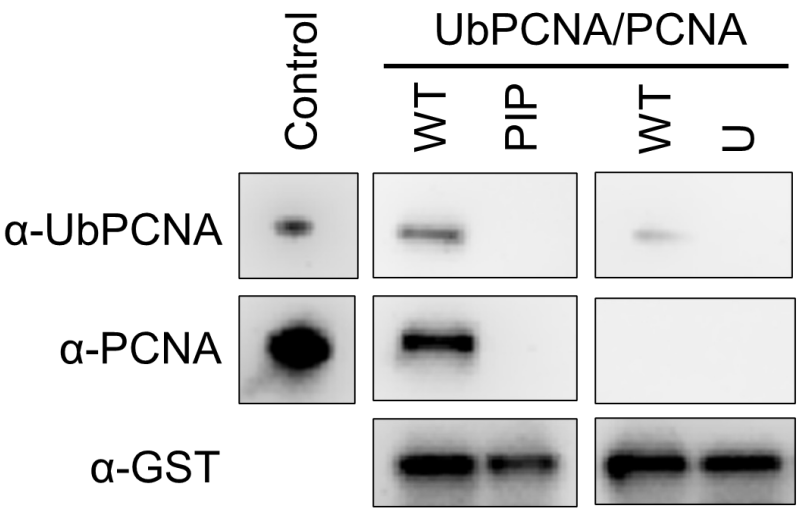

D

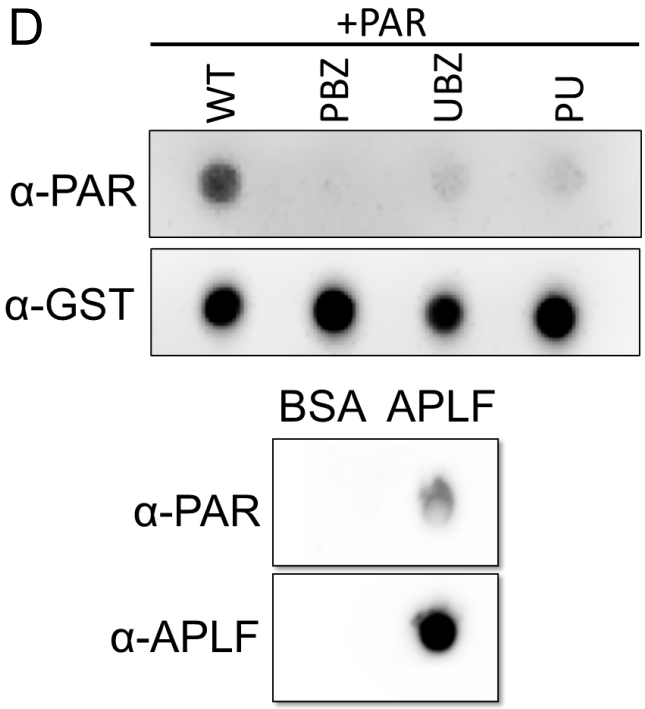

Swift, Figure 4

A

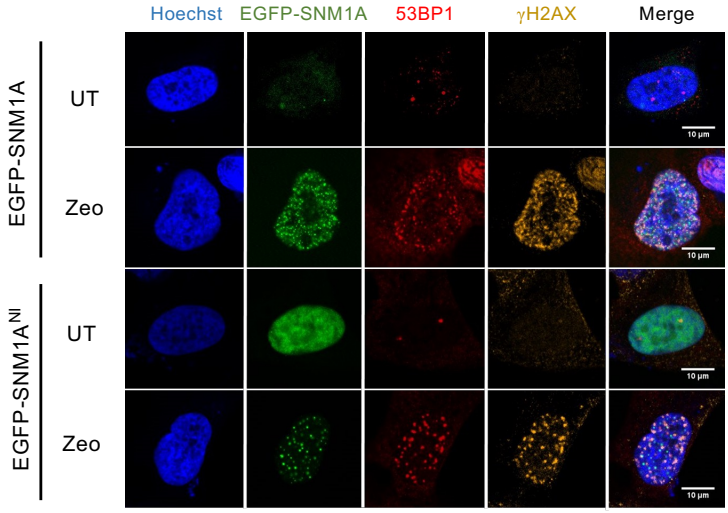

B

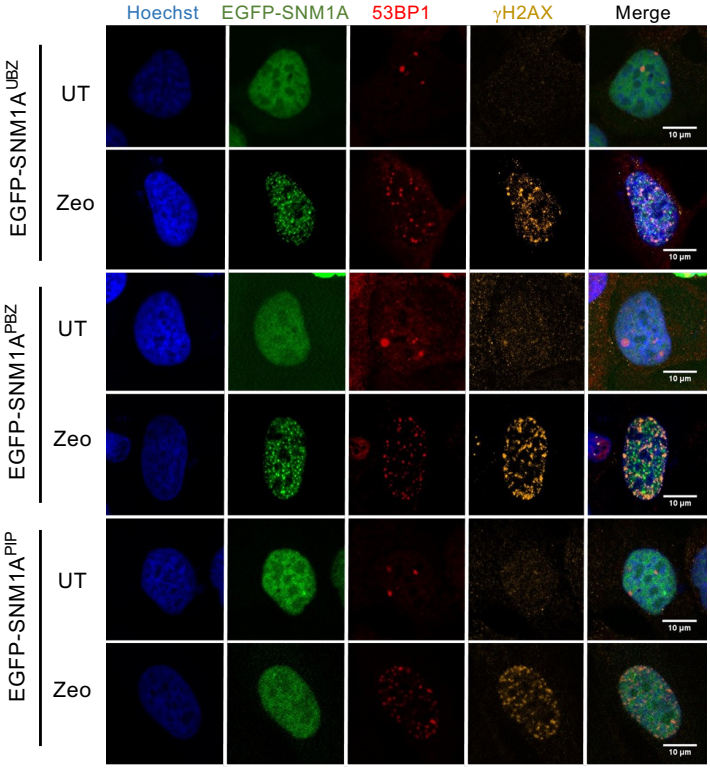

C

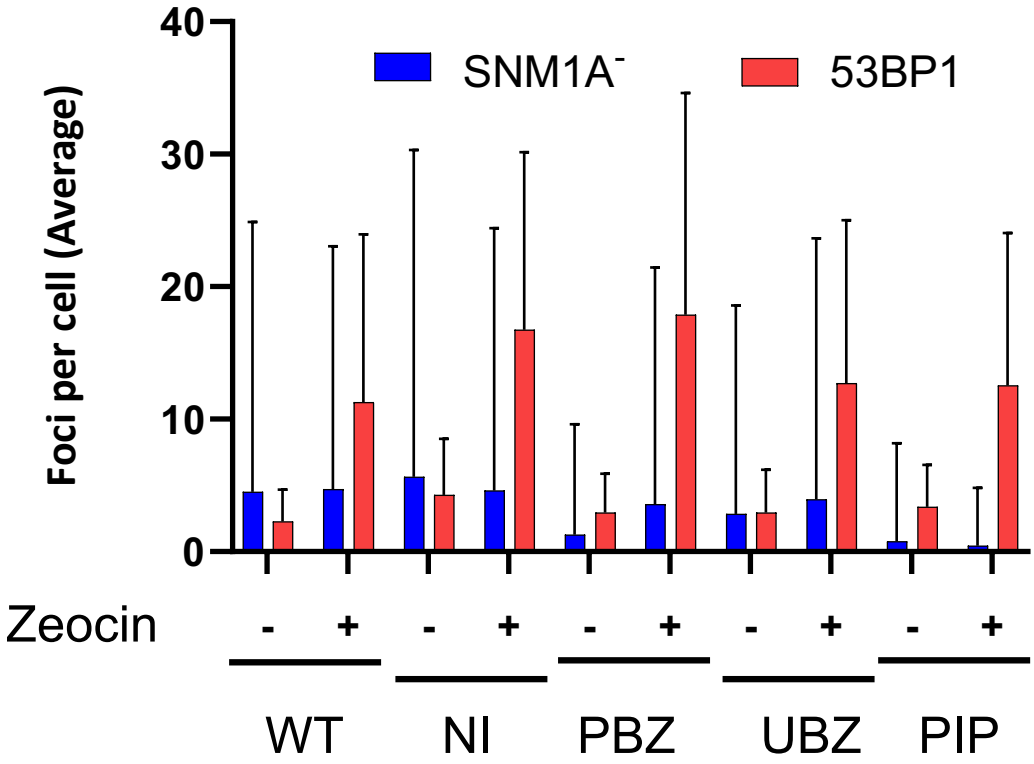

Swift, Figure 5

A

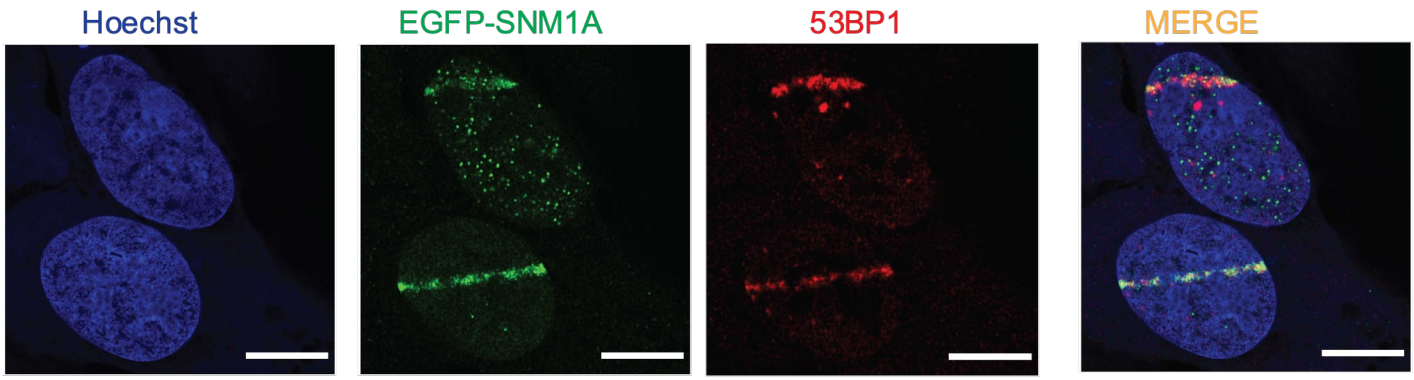

B

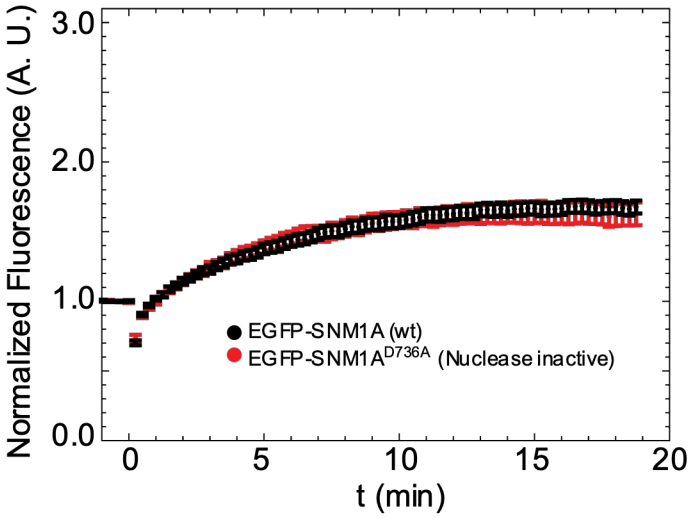

C

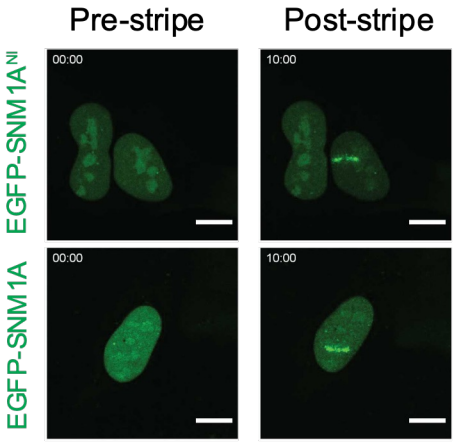

D

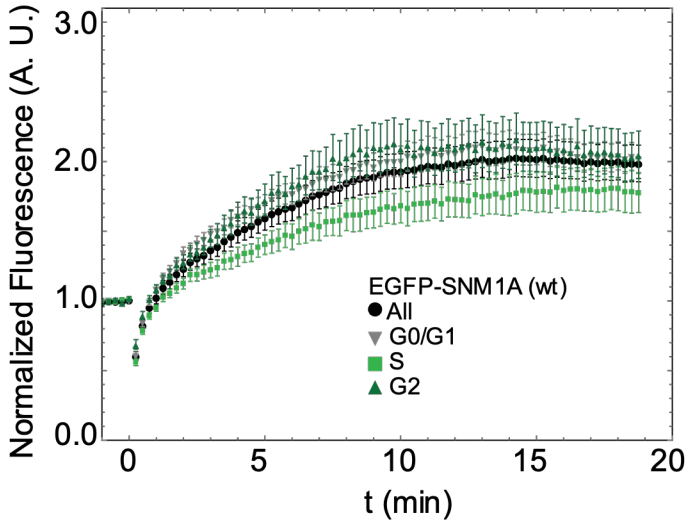

E

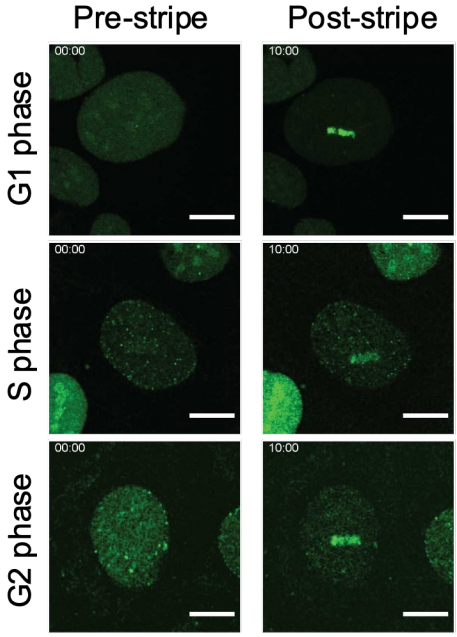

Swift, Figure 6

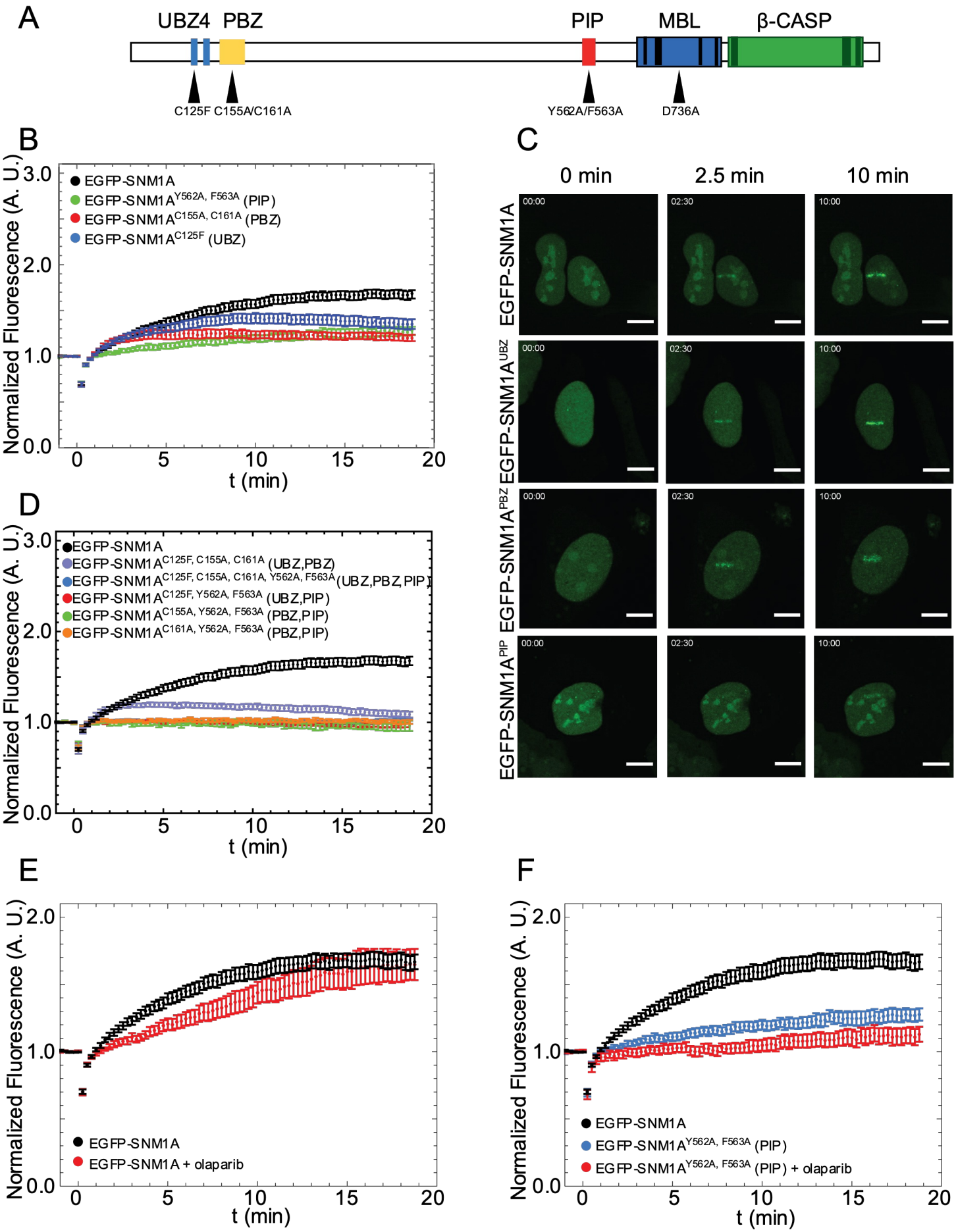

Swift, Figure 7

A

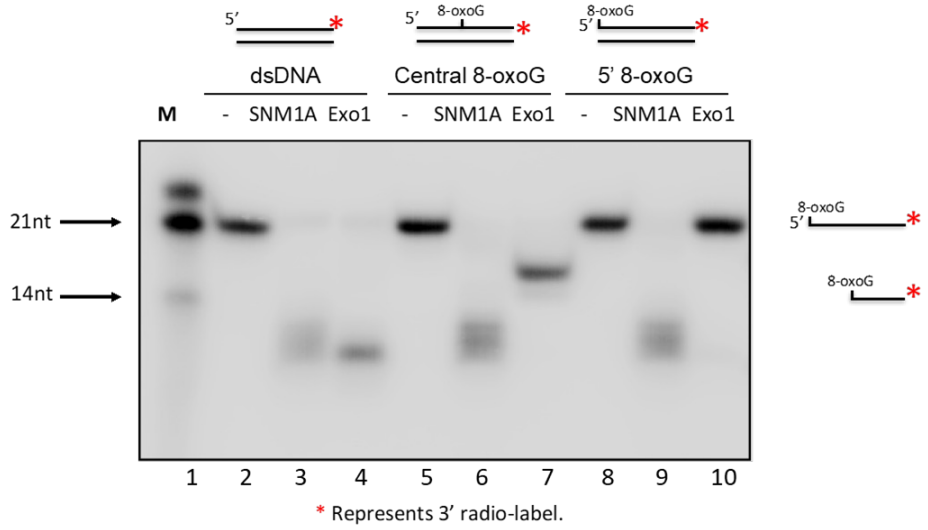
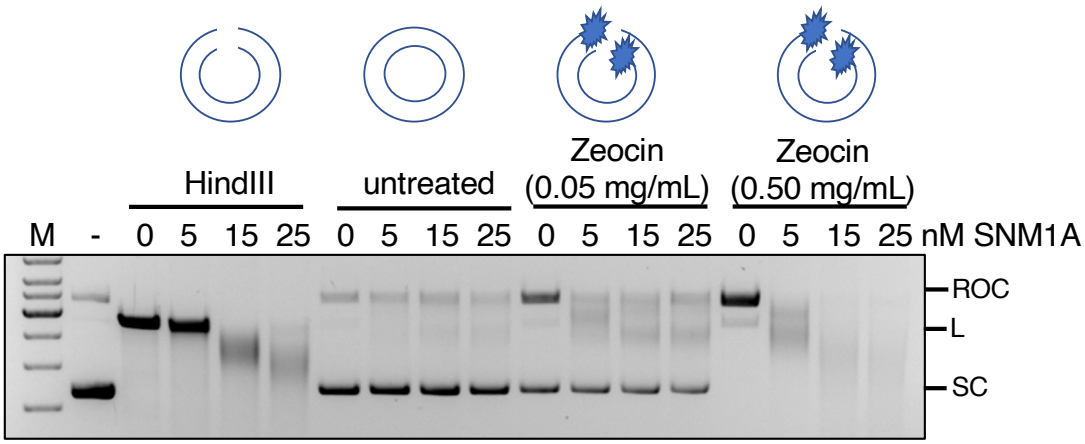
B